

Washington University in St. Louis

## Washington University Open Scholarship

---

All Theses and Dissertations (ETDs)

---

January 2011

### Cellular and Cytoskeletal Responses of Myofibroblasts in Three Dimensional Culture to Mechanical Stretch

Sheng-Lin Lee

*Washington University in St. Louis*

Follow this and additional works at: <https://openscholarship.wustl.edu/etd>

---

#### Recommended Citation

Lee, Sheng-Lin, "Cellular and Cytoskeletal Responses of Myofibroblasts in Three Dimensional Culture to Mechanical Stretch" (2011). *All Theses and Dissertations (ETDs)*. 201.

<https://openscholarship.wustl.edu/etd/201>

This Dissertation is brought to you for free and open access by Washington University Open Scholarship. It has been accepted for inclusion in All Theses and Dissertations (ETDs) by an authorized administrator of Washington University Open Scholarship. For more information, please contact [digital@wumail.wustl.edu](mailto:digital@wumail.wustl.edu).

**WASHINGTON UNIVERSITY IN ST. LOUIS**

**School of Engineering and Applied Science**

**Department of Mechanical Engineering and Materials Science**

Dissertation Examination Committee:

Guy M. Genin, Chair

Elliot L. Elson

Jin-Yu Shao

Srikanth Singamaneni

Stavros Thomopoulos

**CELLULAR AND CYTOSKELETAL RESPONSES OF  
MYOFIBROBLASTS IN THREE DIMENSIONAL CULTURE  
TO MECHANICAL STRETCH**

**by**

**Sheng-Lin Lee**

**A dissertation presented to the School of Engineering and Applied Science  
of Washington University in partial fulfillment of the  
requirements for the degree of**

**DOCTOR OF SCIENCE**

**August 2011**

**Saint Louis, Missouri**

## **ABSTRACT OF THE DISSERTATION**

Cellular and Cytoskeletal Responses of Myofibroblasts in Three  
Dimensional Culture to Mechanical Stretch

by

Sheng-Lin Lee

Doctor of Science in Mechanical Engineering and Materials Science

Washington University in St. Louis, 2011

Research Advisors: Professors Elliot L. Elson and Guy M. Genin

Myofibroblasts play important roles in wound healing and pathological organ remodeling, such as hypertensive cardiac fibrosis and promotion of metastasis. Differentiated myofibroblasts are characterized by increased production of extracellular matrix (ECM) proteins and by the development of  $\alpha$ -smooth muscle actin ( $\alpha$ -SMA) positive stress fibers that are connected to the ECM through focal adhesion assemblies. Moreover, mounting evidence suggests that development of myofibroblasts is profoundly influenced by the mechanical microenvironment, especially, by the structure, organization or stiffness of the ECM (Hinz and Gabbiani, 2003a). Myofibroblasts are likely signaled by mechanical changes in their environment transduced through their cytoskeletons, and the fundamental goal of this dissertation is to develop our understanding of this transduction, with the long term goal of guiding treatments that modulate the responses of myofibroblasts to their mechanical environment.

Previous studies provide a tremendous amount of data for how cells adapt to mechanical stress in two dimensions (2D). Many techniques exist for probing cytoskeletal responses in 2D. These range from pushing cells with a fluid to poking cells with an AFM probe to pulling cells using micropipette aspiration. However, myofibroblasts in a realistic tissue environment cannot be tested using these approaches. The challenge is that cells adopt very different dynamic morphologies in the network of fibers presented by a natural tissue, and cannot be pushed, poked, or pulled using these techniques inside a tissue. The only way to probe the cytoskeleton of such a cell naturally in a tissue is through its natural adhesions to the ECM.

In this work, we developed a 3D tissue culture system to quantify the responses of contractile fibroblasts in an engineered tissue construct (ETC) to external mechanical stimuli. We try to answer the following questions. How does the actin cytoskeleton respond and adapt to mechanical stretch? How does this relate to whole-cell kinematics? How do cells interact with the extracellular environment in 3D?

To address the first question, a suite of mechanical tests were performed on transfected myofibroblasts in ETCs. The transfection enabled the visualization of stress fiber dynamics in 3D, and the work showed for the first time that stress fibers can form in response to mechanical stretch. The work also quantified the diversity of cellular responses into three classes, as described in Chapter 2. To address the second question, we studied the nature of the retraction of filopodium-like processes of stained myofibroblasts in response to mechanical stretch. Results, described in Chapter 3,

showed that retraction of these processes was independent of the magnitude of stretch and the length of the process. The time constants associated with process retractions were very slow compared to membrane retraction in other cells. The study of the last question confirmed that large focal adhesions existed in a 3D environment, early in remodeling, and that focal adhesion complexes evolve during ECM remodeling.

The work in this dissertation helps establish a platform to study cellular mechanics and function in a 3D environment through both real-time imaging and force measurement simultaneously. While the work is at the level of basic biophysics, it provides a quantitative window into the mechanisms underlying myofibroblast-based pathologies.

# Acknowledgments

The work presented here is the culmination of a number of fantastic collaborations with a number of fantastic collaborators. Without their help, my research would be a skeleton of the final results presented in this dissertation.

I would like to express my deep and sincere gratitude to my two research advisors, Elliot L. Elson and Guy M. Genin. Elliot is far more than an excellent and professional biochemist and molecular biophysicist. Elliot's door and arms are always open, and his creative energy is always there to provide insightful opinions and directions for problem solving. Standing on the shoulder of this giant helps me see much farther than I could have otherwise, and provided a totally different point of view. My major advisor, Guy, inspires me to strive for perfection and to excel beyond myself. I am grateful for his motivation and everlasting support. Their enthusiasm, patience, and excellence in academic research, and their hard work and generosity an outstanding example I want to match in the future. I learned during the research work: "do things right, and do the right things."

I would like also thank Kenneth M. Pryse for sharing many thoughtful and creative ideas throughout my experimental adventures. Frustrations and surprises always exist in biological systems and experiments, and with Kenneth's superior guidance, I was able to develop my own risk control and problem solving strategies. When I face these difficulties, I have developed the patience to calm down, assess the situation, and compose tactics for overcoming these difficulties.

I would also like to thank the government of Taiwan government for sponsoring me through a fellowship for graduate study overseas. This full financial support in the early stages of my research was a unique opportunity that allowed me to focus on challenging, interesting, high risk, and high impact research issues.

Finally, and most importantly, I want to thank my parents, Chung-Min Lee and Hsiu-Yun Cheng Lee. Through their love and support, I can always overcome the challenges and problems of not only research work but also of life itself.

**Sheng Lin Lee**

*Washington University in St. Louis*

*August 2011*

This dissertation is dedicated to my parents.



# Table of Contents

<b>ABSTRACT OF THE DISSERTATION</b> .....	<b>II</b>
<b>ACKNOWLEDGMENTS</b> .....	<b>V</b>
<b>TABLE OF CONTENTS</b> .....	<b>VIII</b>
<b>LIST OF TABLES</b> .....	<b>XI</b>
<b>LIST OF FIGURES</b> .....	<b>XII</b>
<b>CHAPTER 1 : INTRODUCTION</b> .....	<b>1</b>
1.1 Overview .....	1
1.2 Outline of the Dissertation.....	1
<b>CHAPTER 2 : MECHANICALLY-INDUCED REMODELING OF THE ACTIN CYTOSKELETON IN A THREE DIMENSIONAL TISSUE CONSTRUCT</b> .....	<b>4</b>
2.1 Introduction.....	5
2.2 Materials and Methods .....	8
2.2.1 Preparation of Engineered 3D Tissue Constructs.....	8
2.2.2 Cell Stretching System .....	10
2.2.3 Experimental Protocols.....	11
2.2.4 Microscopy .....	12
2.3 Results .....	12
2.3.1 Cells in ETCs Adapt Actively to Mechanical Stretch.....	12
2.3.2 Stress Fibers Form in Response to Mechanical Stretch .....	16
2.3.3 Cytoskeletal Rearrangement Occurs Through Three Temporal Sequences .....	18
2.3.4 The Rho Kinase Pathway Is Not Essential to Stress Fiber Formation.....	22
2.3.5 Ensemble-Averaged Active Cellular Contraction Is Independent of Mechanical Stretch.....	23
2.4 Discussion .....	24
2.4.1 Stress fibers and F-actin Patches in Cells Cultured in a 3D Environment Are Sensitive to Mechanical Stimuli .....	24
2.4.2 Cytoskeletal Dynamics in 3D Differ from Those Observed in 2D.....	28
2.4.3 Stress Fiber Formation Does Not Require the Rho Pathway .....	31

2.4.4 Limitations.....	32
<b>2.5 Supplemental Document .....</b>	<b>35</b>
2.5.1 Supplemental Methods .....	35
2.5.2 Supplemental Results .....	36
2.5.3 Supplemental Discussion .....	43
<b>2.7 References: .....</b>	<b>48</b>
<b>CHAPTER 3 : DYNAMICS OF MEMBRANE RETRACTION IN A THREE DIMENSIONAL TISSUE CONSTRUCT .....</b>	<b>51</b>
<b>3.1 Introduction.....</b>	<b>52</b>
<b>3.2 Materials and Methods .....</b>	<b>54</b>
3.2.1 Preparation of Engineered 3D Tissue Constructs.....	54
3.2.2 Testing Device .....	55
3.2.3 Experimental Protocol.....	57
3.2.4 Multidimensional imaging of tissue constructs .....	59
<b>3.3 Results .....</b>	<b>63</b>
3.3.1 Cell Dynamics in the ETCs Can Be Monitored by Membrane Staining.....	63
3.3.2 Cells Change Membrane Morphology in Response to Mechanical Stretch.....	66
3.3.3 Rates of Stretch-Induced Process Retractions Were Stretch-Independent, and Were Faster Than Process Retractions in the Absence of Stretch .....	68
<b>3.4 Discussion .....</b>	<b>71</b>
3.4.1 Cells Respond Actively to Mechanical Perturbation of Their Environment.....	71
3.4.2 A Coupled Imaging and Mechanical Measurement System Can Be Applied to Quantify Cellular Responses to Mechanical Stretch.....	72
<b>3.5 Conclusions .....</b>	<b>76</b>
<b>3.7 References .....</b>	<b>77</b>
<b>CHAPTER 4 : FOCAL ADHESIONS IN THREE DIMENSIONAL TISSUE CONSTRUCTS .....</b>	<b>79</b>
<b>4.1 Introduction.....</b>	<b>79</b>
<b>4.2 Materials and Methods .....</b>	<b>81</b>
4.2.1 Preparation of Engineered 3D Tissue Constructs.....	81
4.2.2 Transfection of GFP-Vinculin .....	82
4.2.3 Microscopic Measurement of GFP-Vinculin .....	82
4.2.4 Fluorescence Photobleaching Recovery (FPR).....	83
<b>4.3 Results .....</b>	<b>85</b>

4.3.1 Larger Focal Adhesions Exist in Tissue Constructs Early in Remodeling .....	85
4.3.2 The Remodeling of Collagen and Cells in ETCs.....	89
4.3.3 FPR Results .....	91
<b>4.4 Discussion .....</b>	<b>96</b>
<b>4.5 References .....</b>	<b>98</b>
<b>CHAPTER 5 : FUTURE WORK.....</b>	<b>99</b>
<b>CURRICULUM VITA.....</b>	<b>103</b>

# List of Tables

Table 4- 1	Type I curve fitting parameters.....	94
Table 4- 2	Type II curve fitting parameters.....	95

# List of Figures

Figure 2- 1	Responses of contractile fibroblasts to mechanical stretch.....	14
Figure 2- 2	Time variation of stress fibers in response to mechanical stretch.....	17
Figure 2- 3	(A)Three classes of responses (B) Variation of morphology .....	21
Figure 2- 4	Cell response was largely independent of cell morphology.....	27
Figure SR- 1	$\alpha$ -actinin staining cells in the ETC.....	36
Figure SR- 2	Typical curve of force relaxation .....	37
Figure SR- 3	Time variation of cytoskeleton in stellate and spindle cells. Time course of changes to the actin cytoskeletons of two cells. ....	38
Figure SR- 4	Time course of fibrosity treated with Y-27632.....	40
Figure SR- 5	Time course of cellular area and perimeter treated with Y-27632.....	41
Figure SR- 6	Force response of cells treated with Y-27632 at different stretch level.....	42
Figure SR- 7	Local strains as a function of the nominal strains on the ETC.....	43
Figure 3- 1	Testing devices and system diagram .....	55
Figure 3- 2	Illustration of image data processing.....	60
Figure 3- 3	Concept of convolution and deconvolution in the fluorescence image .....	62
Figure 3- 4	Star-like(stellate) cell in response to mechanical stretch .....	64
Figure 3- 5	Spindle-like cell in response to mechanical stretch.....	65

Figure 3- 6	Morphological reconstruction of cells in response to the mechanical stretch .....	67
Figure 3- 7	Retraction of plasma membrane and cytoskeleton in response to the mechanical stretch.....	69
Figure 3- 8	Time constants of cellular dynamics in response to mechanical stretch.....	70
Figure 4- 1	Original and corrected FPR curve .....	84
Figure 4- 2	Focal adhesions in button gels.....	85
Figure 4- 3	Immunolabeling of focal adhesions in ETCs.....	86
Figure 4- 4	Comparisons of Focal adhesions between 2D and 3D environment. ....	88
Figure 4- 5	Remodeling of collagen fibers in ETCs .....	90
Figure 4- 6	Collagen remodeling and Connective network of cells.....	91
Figure 4- 7	Type I curve of FPR.....	94
Figure 4- 8	Type II curve of FPR.....	95

# Chapter 1 : Introduction

## 1.1 Overview

Interactions between cells and their mechanical environments are central to understanding a host of physiologic and pathologic events ranging from development to wound healing to metastatic cancer. While much information is known from observations of cells in two-dimensional (2D) culture on substrates ranging from glass to compliant polymers to structured pillars that allow measurement of force, tools are just now becoming available to study cells and their mechanical functioning in realistic three-dimensional (3D) environments. In this dissertation, we explore the ways that cells, including their membranes, focal adhesions, and actin cytoskeletons, react to mechanical stimulus when cells are cultured in a model 3D environment based on collagen that we call “engineered tissue constructs” (ETCs). In addition to contributing fundamental observations that are the first of their kind for cells in 3D environments, the dissertation presents a home-designed stretcher with incorporated with a confocal microscope to monitor and analyze fibroblast dynamics in ETCs.

## 1.2 Outline of the Dissertation

First, in Chapter 2, we investigate the morphology of the actin cytoskeleton in a 3D tissue construct, and how it responds to mechanical stretch. Cells exhibited two classes of response to mechanical stimuli: retraction and reinforcement. "Retraction" responses included retraction of cellular protrusions, depolymerization of actin stress

fibers, and formation and growth of patches of F-actin. "Reinforcement" responses included extension of cellular protrusions, polymerization of actin stress fibers, and disappearance and shrinkage of patches of F-actin. 3D extension of cellular protrusions occurred in predominantly in the direction of applied stretch, consistent with observations of cells in 2D. Contrary to observations of cells in 2D, retraction and reinforcement responses could both be observed at sustained nominal stretches, and occurred independently of cell orientation, cell morphology, and peak principal strain (10% or 30%). Following stretch, some cells exhibited retraction responses followed by reinforcement responses, but no cells exhibited reinforcement responses followed by retraction responses. Results suggest that conditions specific to individual cells govern mechanical responses in a 3D mechanical environment. Results further suggest that stress fibers can form in response to external mechanical stimuli in contractile fibroblasts cultured in 3D ETCs through a passive pathway that is independent of rho kinase, and that transients between stretch-dependent homeostatic states of fibroblasts in 3D culture involve an interplay between F-actin patches and stress fibers.

Second, in Chapter 3, we further investigate how the cell membranes respond to analogous loadings. We studied how membrane morphology changed in response to mechanical loading when ETCs are stretched and held isometrically. Also, we measure the time constants among groups with different mechanical stimuli to understand how those mechanical perturbations modulate the way that cells respond to their environment. The results suggest cells in a mechanically manipulated environment respond slightly differently based upon their morphology. Time constants indicate that



membrane dynamics in response to mechanical stimuli are limited by cytoskeletal features.

Third, in Chapter 4, our experiment results proved the existence of focal adhesions in both button gels and ring shaped ETCs. Qualitative observations suggested that the sizes of focal adhesions varied with the degree of remodeling within ETCs. We measured replacement rates of focal adhesions in 3D environment through fluorescence photobleaching recovery (FPR) experiments.

Finally, in Chapter 5, we describe and compose future work to test the hypothesis that the FA-like structures in Chapter 4 become more dynamic with increased remodeling of the tissue construct in which they are embedded. Our strategy is to measure replacement rates through fluorescence photobleaching recovery (FPR) experiments. We will determine whether remodeling or stiffness is the factor underlying their disappearance by modulating the stiffness of the collagen extracellular matrix.

# **Chapter 2 : Mechanically-Induced Remodeling of the Actin Cytoskeleton in a Three Dimensional Tissue Construct**

Quantifying the response of living cells to mechanical stimuli is important to understanding a great number of physiologic, developmental, and pathologic cellular functions. For example, mechanically-induced cellular responses are thought to be determinants of musculoskeletal healing outcomes and to underlie pathologic remodeling associated with cardiac fibrosis. While much is known about these responses for cells cultured on a two-dimensional (2D) substrate, little is known about mechanical responses of cells in a natural, 3D environment. We developed a system to observe the actin cytoskeletons of contractile fibroblast cells cultured in a 3D collagen-based extracellular matrix that was stretched over the objective of a confocal microscope. Cells exhibited two classes of responses to mechanical stimuli. "Retraction" responses included retraction of cellular protrusions, depolymerization of actin stress fibers, and formation and growth of patches of F-actin. "Reinforcement" responses included extension of cellular protrusions, polymerization of actin stress fibers, and disappearance and shrinkage of patches of F-actin. 3D Extension of cellular protrusions occurred in predominantly in the direction of applied stretch, consistent with observations of cells in 2D. Contrary to observations of cells in 2D, retraction and reinforcement responses could both be observed at sustained nominal stretches, and occurred independently of cell orientation, cell morphology, and peak principal strain

(nominally 5% and 10%). Following stretch, some cells exhibited retraction responses followed by reinforcement responses, but no cells exhibited reinforcement responses followed by retraction responses. Results suggest that stress fibers can form in response to external mechanical stimuli in contractile fibroblasts cultured in 3D ETCs through a passive pathway that is independent of rho kinase. Results further suggest that transients between stretch-dependent homeostatic states of fibroblasts in 3D culture involve an interplay between F-actin patches and stress fibers.

## 2.1 Introduction

Living cells sustain a broad range of mechanical stimuli in physiologic circumstances, but the responses of cells to mechanical stimuli within a natural tissue are poorly understood. Pathologic responses to mechanical stimuli are believed to underlie diseases such as fibrotic cardiomyopathy (Rohr 2009) and asthma (Fredberg 2002). Potentially advantageous cellular responses are the motivation for post-operative rehabilitation protocols applied following tendon-to-bone reattachment surgery (Thomopoulos, Williams et al. 2003). Cellular responses to mechanical stimuli range from cytoskeletal reorganization (Treat, Deng et al. 2007; Nekouzadeh, Pryse et al. 2008; Krishnan, Park et al. 2009) and cellular reorientation (Kaunas, Usami et al. 2006; Zemel, Rehfeldt et al. 2010) to trans-differentiation (Forte, Della Corte et al. 2010) and cell death (Bayly, Dikranian et al. 2006). Emerging evidence suggests that mechanical signals transduced through the actin cytoskeleton and its connections to the extracellular matrix (ECM) have important effects on cell physiology and tissue

development (Geiger, Bershadsky et al. 2001; Vogel and Sheetz 2006; Taber 2009). In each of these cases, the responses of cells to changes in their mechanical environment are important but only partially understood.

We therefore developed a model system to study the responses of the actin cytoskeletons of contractile fibroblasts to mechanical stretch in three-dimensional (3D) tissue culture. The actin cytoskeletons of analogous cells exhibit a range of responses to mechanical stretch. In 2D culture systems, these include cytoskeletal fluidization in response to a single stretch followed by a release (Treat, Deng et al. 2007; Krishnan, Park et al. 2009), and cytoskeletal reinforcement in response to a single sustained stretch (Treat, Deng et al. 2007) or localized stressing (Krishnan, Park et al. 2009). In response to rapid ( $>1$  Hz) cyclic stretching, endothelial cells have been observed to align perpendicular to the direction of stretch, and in response to slower cyclic stretching, these cells have been observed to align parallel to the direction of stretch (De and Safran 2008; Kaunas and Hsu 2009; McGarry 2009). However, cells in 2D culture systems differ morphologically from those in natural tissues, and the focal adhesion assemblies hypothesized to underlie signaling in force transduction are rarely observed in 3D culture or in natural tissues.

In 3D culture systems, contractile fibroblasts have been observed to display a fluidization followed by reinforcement to pre-stretch levels in response to a rapidly

applied sustained stretch (Nekouzadeh, Pryse et al. 2008). However, these data for cytoskeletal dynamics are taken from fixed cells at sparse time points, and individual cells could not be distinguished. We hypothesized based upon these earlier observations that individual contractile fibroblast cells in 3D tissue constructs would respond to mechanical stretches through remodeling at the cellular and cytoskeletal levels.

By stretching engineered tissue constructs (ETCs) over the objective of a confocal fluorescence microscope, we observed two classes of cytoskeletal responses to isometric stretching of the ETC: retraction responses, involving retraction of cellular processes, depolymerization of actin stress fibers, and formation and retraction of F-actin patches, and reinforcement responses, involving extension of cellular processes in the direction of applied stretch, formation of stress fibers in the direction of applied stretch, and decreases in the size and number of the F-actin patches. Cells were cultured with a density that ensured the final ETCs would reach the cell concentration associated with the percolation threshold, at which cell and ECM moduli are believed to be in registry and at which the stress field within the ETCs is believed to be most uniform (Marquez, Genin et al. 2006; Marquez, Elson et al. 2010). To visualize cytoskeletal dynamics, a fraction of cells were transfected with m-cherry LifeAct, an F-actin reporter. Results demonstrate that cells respond with both "retraction" and "reinforcement" responses to mechanical stretches, and that these responses were not well predicted by the initial orientation or morphology of the cells, or by the degree of stretch (5% or 10%) of the tissue construct. Some cells exhibited retraction responses

followed by reinforcement responses, but the opposite never occurred. Results indicate that stress fibers form in response to external mechanical stimuli in contractile fibroblasts cultured in 3D ETCs through a passive pathway that is independent of rho kinase. Results suggest that stress fibers form in response to external mechanical stimuli in contractile fibroblasts cultured in 3D ETCs through a passive pathway that is independent of rho kinase, and that transients between stretch-dependent homeostatic states of fibroblasts in 3D culture involve an interplay between F-actin patches and stress fibers.

## **2.2 Materials and Methods**

### **2.2.1 Preparation of Engineered 3D Tissue Constructs**

Chicken embryo fibroblast (CEF)-populated collagen-based engineered tissue constructs (ETCs) were synthesized to provide a realistic 3D environment in which to probe the effects of mechanical stimulus on cytoskeletal dynamics. ETC synthesis built upon a protocol reported elsewhere (Wakatsuki et al, 2000), but fluorescent microspheres were added to the collagen gel ECM, and certain percentages of cells were transfected with a fluorescent protein that allowed for visualization of F-actin. CEFs isolated from 10-day chicken embryos (fertile white leghorn chicken eggs, Sunrise Farms, Catskill, NY) were maintained in Dulbecco's modified Eagle's medium (DMEM) with 10% fetal calf serum (FCS), penicillin and streptomycin at 50 units/ml and 50  $\mu$ g/ml respectively, and without phenol red, a pH indicator.

Approximately 5% to 10% of the cells were transfected with the F-actin reporter m-cherry LifeAct. The LifeAct peptide associates with actin filaments without affecting cellular dynamics. To ensure that the transfection was not toxic to cells, comparisons were made between populations of transfected and untransfected cultures over periods of 5 days; no significant trends in proliferation or viability were observed relative to controls.

The CEFs in 10% FCS DMEM were then combined with home-made monomeric type I rat tail collagen dissolved in 0.02 M acetic acid, neutralized if necessary at 4°C with 0.1 M NaOH. Concentrated DMEM was also added to the mixture to yield a final collagen content of 1 mg/ml. Fluorescent carboxylate microspheres (#17156, Polysciences Inc., Warrington, PA), 5.707  $\mu\text{m}$  in diameter, were added to the cell/collagen suspension at a final concentration of  $3.55 \times 10^3$  particles/ml. Neutralized solutions were composed of collagen (1.0 mg/ml) with a cell density of  $10^6$  cells/ml. The solution was poured into annular molds (7.92 mm inner diameter, 19.0 mm outer diameter). After three days of culture, over which the cells actively remodeled and compressed the collagen solution, and ring-shaped ETCs (approximate dimensions: 5 mm inner diameter, 8mm outer diameter, 6 mm height) were removed from the inner mandrel of the molds and mounted on the custom designed stretcher for testing.

## 2.2.2 Cell Stretching System

To simultaneously measure ETC force responses and monitor cellular responses inside uniaxially stretched ETCs, a custom-made tissue stretcher was designed to work over a confocal microscope. The stretcher consists of three major subassemblies: an isometric force transducer, a mounting stand, and a linear actuating stepper motor. The isometric force transducer (model 724490, Harvard Apparatus, Holliston, MA) connects to the one end of the tissue through a titanium mounting rod, and the linear actuating stepper motor to the other through a second titanium mounting rod. The linear actuating stepper motor has a resolution of 1.5  $\mu\text{m}$  per step. To make the device capable of moving with a tolerance of less than 1.0  $\mu\text{m}$ , an eighth-stepping driver (custom developed by Gavin Perry, Washington University Electronics Shop) is used. Since the stepper motor was unipolar, the card manipulates the current to each transistor causing the electromagnets to turn the motor only one eighth of a step. We used a computer with custom-made software in the Experix environment operating on a Linux-based operating system to send signals through the digital I/O channels of a PCMCIA card (model DAS16/16-AO, Measurement Computing, Norton, MA) to the stepper motor via the eighth-stepping driver. The software also acquired force data from the force transducer through the same card. Scripts were written for two stretching protocols: a cyclic stretch, used for preconditioning stretch, and a rapid step stretch followed by an isometric hold, in which tissue constructs were quickly lengthened then held at that length while the force was monitored for 30 minutes.



### 2.2.3 Experimental Protocols

The mechanical response of cells to stretch was measured as cell morphology was tracked using confocal fluorescence microscopy. After the ETC was mounted, the imaging system was refocused to locate stained cells within the ETC to monitor dynamic activity before and following stretching of the ETC. The stretching protocol was 10% preconditioning stretches applied at 20%/s, followed by a 10% stretch at 60%/s and an isometric hold for thirty minutes while force and imaging data were acquired. This was followed by a 30% stretch and an isometric hold for an additional 30 minute interval of force and imaging data acquisition. ETCs were kept at 37°C in on a heated micro-incubator stage.

Y-27632 has been widely used as a Rho-associated kinase (ROCK) inhibitor to identify and evaluate the involvement and roles of ROCK kinases in many biological phenomena, including wound healing, cardiomyocyte hypertrophy, and bronchial smooth muscle contraction. To better understand the dynamics of fibroblasts in response to external mechanical stimuli, we studied cellular responses in some ETCs treated with 10  $\mu$ M Y-27632. To study effects of internal stores of  $\text{Ca}^{2+}$ , some specimens were treated with thapsigargin to release internal stores of  $\text{Ca}^{2+}$  (Thastrup, Cullen et al. 1990), and then with BAPTA AM to chelate the internal  $\text{Ca}^{2+}$ .

## 2.2.4 Microscopy

Following mounting of ring-shaped ETCs onto the stretcher, the ETC and stretcher were placed over the objective of a confocal fluorescence microscope. Imaging was done using a long working distance 20X objective and all multidimensional images were taken by on a Ziess confocal laser scanning microscope (Axiovert 200M with LSM 510 ConfoCor 2, Carl Zeiss Inc., Oberkochen, Germany) with fluorescence excited by a helium-neon laser. All images were acquired with 10-bit resolution. The imaging protocol involved tracking the reconfiguration of cells with a stack of confocal microscopy images taken through the cell thickness every 5 minutes.

## 2.3 Results

### 2.3.1 Cells in ETCs Adapt Actively to Mechanical Stretch

Cells in the ETCs exhibited filopodia-like protrusions in the ECM that extended and retracted continuously (Supplemental Movie 1). Prior to mechanical stimulus most cells displayed a diffuse cytoskeleton composed of a random arrangement of actin filaments, and a few cells contained visible stress fibers (cf. Fig. 1A, label 1) or aggregations of actin "patches" (cf. Fig. 1A, label 3). Actin patches were shown by staining for  $\alpha$ -actinin to contain F-actin (Supplemental Results, Figure SR-1). In response to mechanical stretch, the force necessary to maintain the tissue constructs isometrically increased from the baseline pre-stretch value. The isometric force then decreased to slightly above the baseline pre-stretch value over the course of

approximately 30 minutes, as the ECM and cells relaxed viscoelastically and as the cells remodeled actively (Supplemental Results, Figure SR-2).

During this time, cells exhibited two broad classes of responses (Fig. 1, time courses available in Supplemental Movies 2 and 3). "Retraction" responses included three phenomena. First, cellular protrusions retracted, independent of their orientation (Fig. 1, label 1). Second, stress fibers depolymerized (label 2). Third, the F-actin patches (label 3) grew in size, and some new patches were observed, often near the site of retraction of cellular protrusion retraction or stress fiber depolymerization. "Reinforcement" responses included extension of cellular protrusions (label 4), polymerization and thickening of actin stress fibers (label 5), and disappearance and shrinkage of F-actin patches (label 6), often near the site of the extension of cellular protrusions. Extension of cellular protrusions occurred in predominantly in the direction of applied stretch (Fig. 1C).

Two magnitudes of stretch were applied to cells, nominally 5% and 10%; because of the bimodal elastic behavior of collagen the structure of the ETCs, this required 10% and 30% nominal stretches of the distance between the points of force application, respectively (see Discussion). An independence of  $\chi^2$  test performed to identify relationships between magnitude of mechanical stretch (5% and 10%) and filopodial responses (extension, no response, and retraction) showed that filopodial responses were related to mechanical stretch ( $\chi^2=7.33$ ,  $P(>\chi^2)=0.03$ ). Although cells in the control group (no mechanical stretch) changed over the 30 minute observation, all

three classes of filopodial responses were equally likely in the control group (Fig. 1C). Results suggest that contractile fibroblasts responded actively to a uniaxial mechanical stretch and that the degree of mechanical increased the tendency of cells to exhibit retraction responses.

Test protocols were designed to monitor the same transfected cell at different degrees of stretch. After unloading and mechanical relaxation, cells were subsequently stretched 10%, with qualitatively identical classes of cell responses (Supplemental Movies 3 and 4).

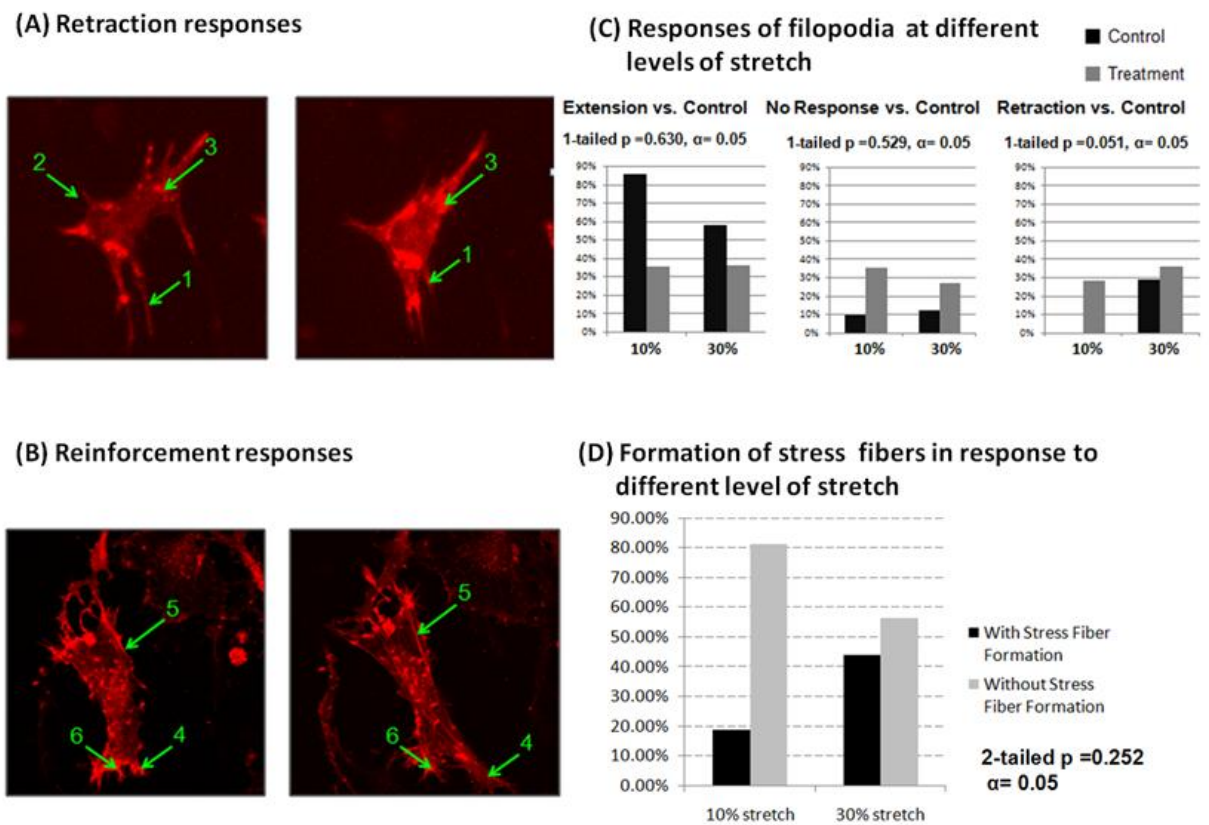


Figure 2- 1 Responses of contractile fibroblasts to mechanical stretch.

A fraction of contractile fibroblasts in a 3D tissue construct were transfected with mCherry-LifeAct (red) prior to being mixed with collagen and incubated for three days. Cells are shown after preconditioning (left), and then in a stretched state (right), 30 minutes after rapid application of a sustained 5% stretch. (Movies of time courses are available as Supplemental Movies 1 and 2). Cells exhibited two classes of responses to mechanical stimuli. "Retraction" responses (A) included: retraction of cellular protrusions (label 1), depolymerization of actin stress fibers (label 2), and formation and growth of patches of F-actin (label 3), often near the site of (1) or (2). "Reinforcement" responses (B) included: extension of cellular protrusions (label 4), polymerization of actin stress fibers (label 5), and disappearance and shrinkage of patches of F-actin (label 6), often near the site of (4) or (5). Extension of filopodia-like cellular protrusions occurred predominantly in the direction of applied stretch. Retraction and reinforcement responses could both be observed following sustained stretches, and occurred independently of cell orientation, cell morphology, and peak principal strain (5% or 10%). (C) Fisher's exact test indicated that the probabilities of inactivity, retraction, or extension of filopodia-like cellular processes were not significantly different compared to control; however, when processes were extended or retracted, the dominant trend was towards extension into the direction of stretch. Process retraction was more likely to occur with higher stretch magnitude. (D) While mechanical stretch was only a weak predictor of the occurrence of stress fiber formation ( $p=0.252$ ), stress fiber formation was more likely with increasing stretch amplitude.

### 2.3.2 Stress Fibers Form in Response to Mechanical Stretch

Formation of stress fibers was observed with following mechanical stretch, although results were independent of strain level ( $p=0.25$ , Fig. 1D). Retraction and reinforcement responses could both be observed during sustained stretches, and occurred independently of cell orientation, cell morphology, and peak principal strain (5% or 10%). To quantify these observations, time series video recordings were acquired of cells within stretched tissue constructs during isometric conditions immediately following application of the stretch, with confocal image stacks obtained over the entire cell every five minutes for 30 minutes.

Some cells exhibited retraction responses followed by reinforcement responses. The spindle cell shown (Fig. 2A) had visible and well-structured stress fibers before stretch. After stretch, the length of the spindle cell decreased in the stretch direction and the projected area of the cell therefore diminished. Immediately following stretch, the sizes of actin patches increased near the polar ends of the cell. During subsequent reinforcement, stress fibers became larger in diameter and new stress fibers formed (Fig. 2B). As can be seen from subtraction images, the process of remodeling and generating stress fibers propagated from one apex of the spindle cell to the whole cell body (Fig. 2B). Additionally, incremental additions of F-actin on the stress fibers occurred exhibited a spaced, striated pattern. These dynamic results suggest that stress fibers within contractile fibroblasts responded dynamically and non-uniformly. Mechanical stretch resulted in continuous cytoskeletal remodeling, whole cell contractility, and

enhanced assembly of stress fibers. Although spatial non-uniformity was observed, no distinction analogous to that between the dorsal and ventral stress fibers observed in 2D culture was evident (Supplemental Discussion, section SD-1).

The spindle-shaped cell of Fig. 2 began and ended the stretching protocol with stress fibers aligned with the direction of mechanical stretching. For stellate cells that did not exhibit such alignment before stretching, cytoskeletal rearrangement demonstrated a tendency to redirect stress fibers parallel to the direction of external mechanical stimulus (Supplemental Results, section SD-3).

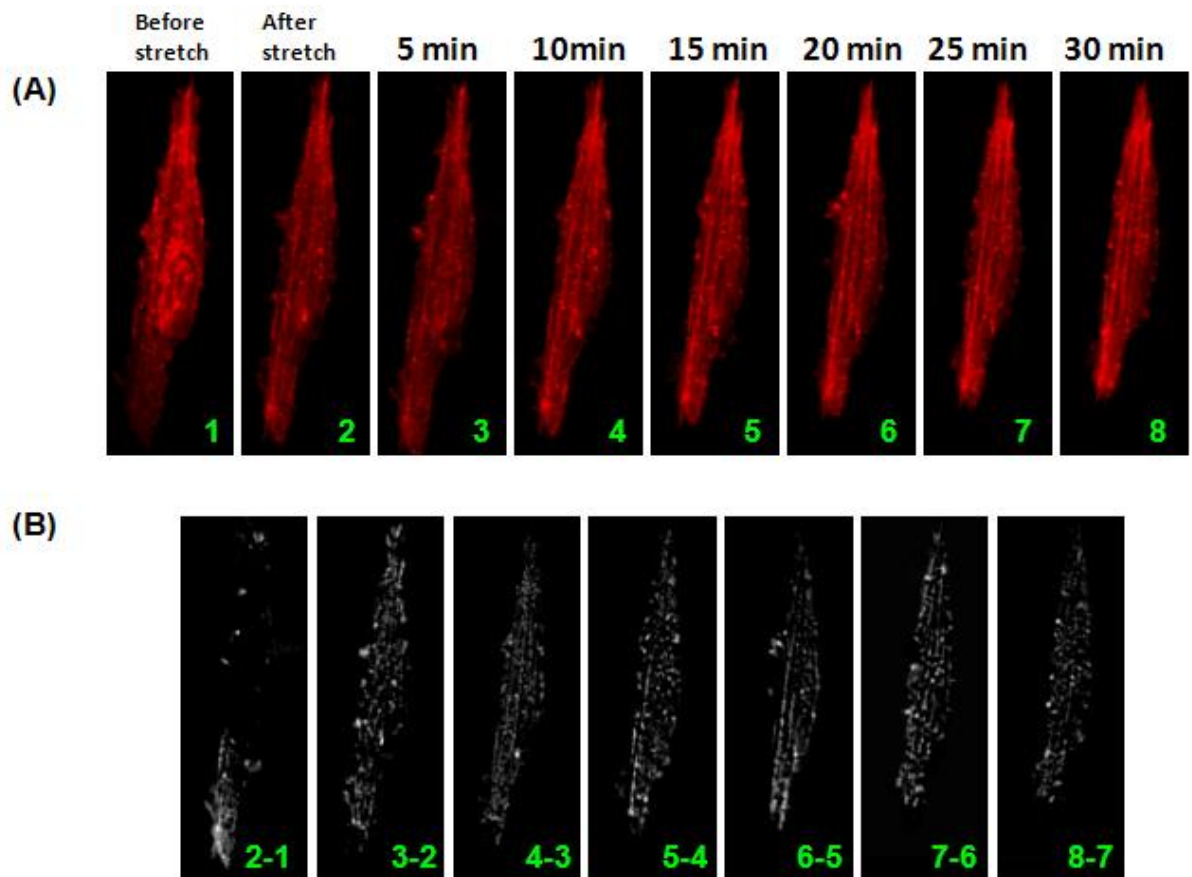


Figure 2- 2 Time variation of stress fibers in response to mechanical stretch

Time series showing partial fluidization followed by reinforcement and formation of actin stress fibers in response to mechanical stretch. (A) Following stretch, the actin cytoskeleton fluidized partially, but stress fibers appeared and were reinforced over the 30 minutes of monitoring. The cell pictured contracted as reinforcement occurred, shortening in length along the stretch direction. (B) Formation and reinforcement of stress fibers is evident from subtraction images involving differences in image intensities of subsequent images (e.g. “2-1” represents the subtraction of image 1 from image 2). Images were aligned prior to subtraction using standard techniques.

### **2.3.3 Cytoskeletal Rearrangement Occurs Through Three Temporal Sequences**

Quantitative stereologic measures were analyzed to quantify these effects. Area and perimeter were studied to analyze morphological changes at the cellular level. Cytoskeletal reorganization was quantified by comparing cellular area to the total length of possibly curved lines of a prescribed thickness range appearing within a projected stack of confocal images using the FABLE technique (Nekouzadeh and Genin, 2011) through a metric termed fibrosity.

Three classes of dynamic cytoskeletal response were evident from confocal image time courses (Fig. 3A). The first was monotonic reinforcement, in which stretch-induced cytoskeletal remodeling led to an increase in fibrosity to a sustained level that was above the pre-stretch level. Amongst these cells, fibrosity increased while the ETC



was stretched to an asymptotic value that was 40-60% higher than its initial values, indicating that the actin cytoskeletons of these cells contained up to 40-60% more F-actin following stretch; note that the upper bound on the passive increase in fibrosity associated with a strain is equal to the strain level. Following 10% stretch, fibrosity increased approximately 50%. These measures were all statistically significant ( $p < 0.05$ ) relative to the control specimens, which were neither pre-conditioned nor stretched; in the control specimens, the normalized standard deviation in fibrosity was 50% of the initial value of fibrosity. However, since the band-pass filtered Fourier transforms used to calculate fibrosity include information about cell perimeters in addition to information about stress fibers, the fibrosity estimates have to be recognized as upper bounds on the stretch-induced increase in F-actin. Estimates of cell area and perimeter must be assessed to determine the degree to which stress fibers contribute to these measures. This is discussed below.

The second class was monotonic retraction, involving fluidization of cytoskeletal structures following stretch, with no recovery. In this group, fibrosity dropped on the order of 20% following 5% stretch, and on the order of 20-40% following 10% stretch. The third group exhibited retraction followed by reinforcement, which appeared in the fibrosity measure as a prompt fibrosity decrease followed by a gradual increase to a peak, sustained level near to or higher than that attained by cells exhibiting only reinforcement. Although for cells exhibiting this class of response the average final values of fibrosity were higher following the 10% stretch than they were following 5%, this was not significant statistically.

Changes in gross cell shape and the contribution of filopodial dynamics were quantified through estimates of variations of area and perimeter of cells following stretch. Because of anisotropy in the specimens, negligible passive area change is expected following stretch; all changes to area can be attributed to cellular remodeling or mechanical changes within cells (Supplemental Document, section SD-2). The data for area changes, averaged over all cells studied ( $n = 16$  cells that were studied at both 5% and 10% stretch levels) indicate rapid response followed by slower reduction over the course of active remodeling, with increases of area greater following 10% stretch than following 5% stretch. The area reduced in both cases to approximately the pre-stretch levels, but did so faster for the lower stretch magnitude.

Perimeter changes were more difficult to interpret because of the contributions of cellular processes, which simultaneously stretched, retracted in directions nominally perpendicular to stretch, and extended in directions nominally parallel to stretch (Supplemental Discussion, section SD-2). Retraction seems to have dominated following 5% stretch, and the perimeter dropped by approximately 10% on average (Fig. 3B). Following the 10% stretch, the perimeter changes nearly paralleled the area changes, suggesting that perimeter changes were dominated by changes to the cell body, and that subsequent retraction and extension of cellular processes occurred in parallel with the mechanisms underlying area change as both area and perimeter returned to approximately their pre-stretch values. These features indicated filopodia were sensitive to the mechanical stretch.

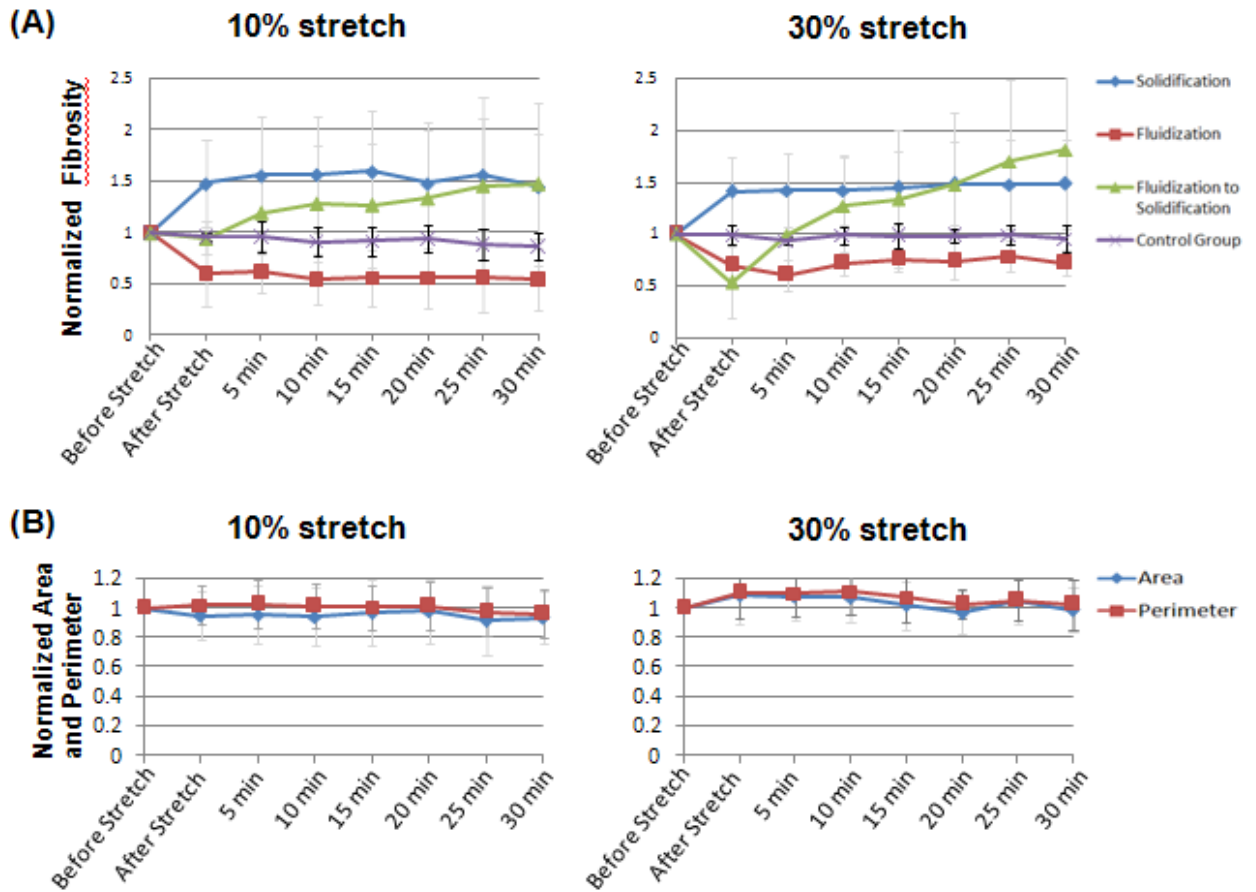


Figure 2- 3 (A) Three classes of responses (B) Variation of morphology

Quantification of cytoskeletal remodeling responses and whole-cell morphological changes as a function of the degree of mechanical stretch. To identify changes in the actin cytoskeletons of cells exposed to the mechanical stretch, changes in the total length of features with the thickness range of stress fibers ("fibrosity") was tracked, as were the area and perimeter of cells. Fibrosity included a measure of the total length of stress fibers in the cytoskeleton, added to a measure of the perimeter of the cell. Area measurements represented a quantitative estimate of cell morphology. (A) Cytoskeletal remodeling at different levels of mechanical stretch (5% and 10% stretch) in different

cells showed reinforcement responses (circles), retraction responses (squares), and retraction followed by reinforcement (triangles); all of these responses were significant compared to the control group that was preconditioned but not stretched (crosses). Each curve represents the average of at least three cells. (B) In nearly all cells studied, the changes in fibrosity were much greater than changes in overall cell morphology. Changes in perimeter were slightly more pronounced at 10% ETC stretch, and changes in area and perimeter were more closely related at 30% ETC stretch; however, neither was large compared to control (Supplemental Results, Fig. SR-5). Each curve represents the average of at least three cells.

### **2.3.4 The Rho Kinase Pathway Is Not Essential to Stress Fiber Formation**

To assay the signaling underlying mechanical induction of stress fibers and preferred directions of process extension and retraction, we modulated intracellular and extracellular  $\text{Ca}^{2+}$  and rho kinase (ROCK). In stretched ETCs in which extracellular  $\text{Ca}^{2+}$  was depleted using thapsigargin and intracellular  $\text{Ca}^{2+}$  was depleted using BAPTA AM, stress fibers failed to regenerate. Although no change in the rates of extension and retraction of filopodia-like extensions was evident in the absence of intra- and extracellular  $\text{Ca}^{2+}$ , these extensions did not show the patterns of preferential extension along the stretch direction or retraction transverse to the stretch direction.

On the contrary, cytoskeletal responses were unaffected by inhibition of the ROCK in stretched ETCs treated with 10  $\mu$ M Y-27632, a rho kinase inhibitor. Stress fibers formed in response to a 30% stretch of the ETC (Supplemental Movie 5) even in cells treated with Y-27632, and fibrosity measurements increased accordingly (Supplemental Results, Fig. SR-4); in the cells studied ( $n=4$ ), fibrosity did not increase following a 10% stretch of the ETC. Cellular area increased by approximately 10% following the 10% ETC stretch but decreased approximately 5% after 30% ETC stretch, indicating that cells were able to alter their morphology after treatment with Y-27632 (Supplemental Results, Figure SR-5). Since these changes are too small to account for observed changes in fibrosity, they further support the assertion that increases in fibrosity were due to stress fiber formation. Taken as a whole, results suggested that the ROCK pathway was not involved in cytoskeletal reorganization or cellular sensing of the mechanical environment, or that an alternative pathway exists for this.

### **2.3.5 Ensemble-Averaged Active Cellular Contraction Is Independent of Mechanical Stretch**

To assess whether active stresses exerted by cells changed in response to ETC stretch, active stresses were estimated in experiments in which ETCs stretched and then held isometrically were treated with Y-27632 (Supplemental Results, Fig. S6-3), which selectively inhibited active stresses by inhibiting the ROCK pathway. By treating a stretched ETC with Y-27632 after a time interval sufficient to allow for viscoelastic relaxation, subsequent changes in isometric force could be associated with changes in

the magnitude of active stress. Following a 5% stretch (Supplemental Results, Fig. S6-3A), the force decrease associated with Y-27632 treatment was approximately  $F_{5\%} = 106\mu\text{N}$ ; following 10% stretch, the decrease was approximately  $F_{10\%} = 105\mu\text{N}$ . Using a linear model to estimate area changes, the active cellular stress following the 5% stretch was estimated as  $\sigma_{0(5\%)} = 116\text{Pa}$  while the estimated stress following 10% stretch was  $\sigma_{0(10\%)} = 119\text{ Pa}$  (Supplemental Results, section SR-4). This suggests that the magnitude of active cellular contraction was independent of the magnitude mechanical stretch in ETCs, consistent with earlier observations (Wakatsuki, Kolodney et al. 2000).

## 2.4 Discussion

### 2.4.1 Stress Fibers and F-actin Patches in Cells Cultured in a 3D Environment Are Sensitive to Mechanical Stimuli

Stress fibers are commonly seen in fibroblasts cultured in 2D substrates, but they are thought to occur very infrequently in connective tissue, and their role in tissues is uncertain (Pellegrin and Mellor 2007). In a 3D ECM, cell shape is largely bipolar and cytoskeletal organization is not clear, frequently lacking discrete focal contacts and stress fibers (Friedl and Brocker 2000). We found that some, although not all, fibroblasts in ETCs generated stress fibers in response to a transient stretch. Before preconditioning, few transfected cells displayed stress fibers; stress fibers might have been absent in these cells throughout culture, or might have disappeared following release from the inner mandrel of the culture molds prior to mounting on the stretching device. Like stress fibers in 2D, stress fibers that we observed in 3D contained irregularly spaced  $\alpha$ -actinin,

and were associated with what appeared to be dominant directions of mechanical stressing.

Unlike stress fibers in 2D, those we observed were not of distinct classes based upon subcellular locations including ventral stress fibers, dorsal stress fibers and transverse arcs (Small, Rottner et al. 1998). An additional distinction of actin stress fiber dynamics in a 3D ETC is that actin patches of diverse sizes are a predominant F-actin cytoskeletal feature. These patches and the stress fibers reorganize within the cytoskeleton in response to mechanical stretching, often in a way that altered gross cell shape towards spindles aligned with the direction of stretch. Patches tended to disappear when stress fibers formed, and to appear when stress fibers disappeared. Patches were also associated with the dynamics of filopodia-like cellular processes.

At the single cell level, the stretch-induced formation of stress fibers in the ETCs was not well predicted by level of mechanical stretch or cell morphology, as highlighted by two examples (Fig. 4). The spindle cell in Fig. 4A initially presented organized and structured stress fibers almost parallel to the stretch direction. Following 5% stretch, some well-organized stress fibers persisted as fibrosity exhibited rapid fluidization followed by gradual recovery to its initial level (Fig. 2), combined with shortening of the cell as a whole; this is evident in the slight drop in fibrosity towards the end of the time course. The aligned spindle cell's well-organized and possibly higher pre-tensioned cytoskeleton might have been particularly well-suited to resist external stimulus. However, following a 10% stretch, the cell again fluidized and recovered

partially, but never regained its initial structure. The apparent transition point at 5-15 minutes following stretch was evident in many cells, and in some cases was associated with cellular contraction; it might also indicate an overshoot as the cell adapted to its new mechanical environment, or an active response to slower stretch-induced changes to the ECM. A stellate cell (Fig. 4B) exhibited both of these responses, but in reverse order. Following 5% stretch, this cell's initially random and non-organized cytoskeleton exhibited rapid fluidization followed by a short rise and a slow decay in fibrosity. However, following 10% stretch, the rapid fluidization was followed by significant reinforcement to a value much larger than the initial fibrosity.

At the tissue level, cellular responses were variable, and we argue that this may arise from difference in cellular microenvironments. Minor variations in microenvironment may be important in both the cellular response to stretch and the pre-stretch configuration of intracellular cytoskeletal structures. A broader dataset allowing a better statistical analysis of cytoskeletal responses (reinforcement, retraction, or retraction followed by reinforcement) would be interesting and informative, and might allow more accurate relation of cytoskeletal response to measured ETC mechanics.



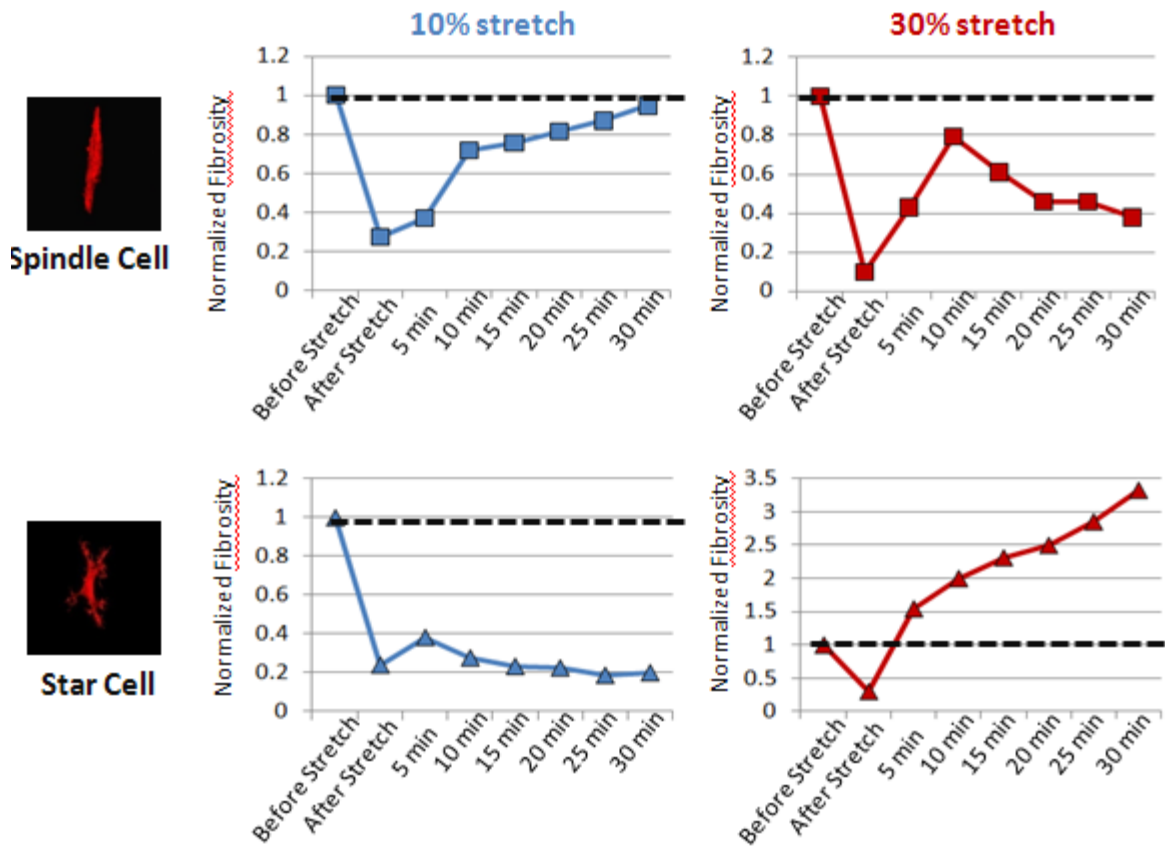


Figure 2- 4 Cell response was largely independent of cell morphology.

The spindle cell aligned with the stretch direction shown in Figure 2 (A) exhibited a retraction response followed by a followed by a reinforcement response following 10% stretch, and a sustained retraction response following 30% stretch. A stellate cell in a nominally identical tissue construct (B) exhibited sustained retraction following a 10% stretch, and a retraction response followed by a reinforcement response after 30% stretch. Technically, we cannot measure the pretension in the cell cytoskeleton. However, the fibrosity of spindle cell with organized stress fibers parallel to the stretch direction was never able to back the initial fibrosity before the rapid stretch. And the fibrosity of star-like cell with diffused f-actin was able to respond to the higher

magnitude of stretch and demonstrated 3 fold of fibrosity in response to the higher stretch. These results might be consistent with the ideas of maximum and minimum pre-tension in the cell cytoskeleton.

## **2.4.2 Cytoskeletal Dynamics in 3D Differ from Those Observed in 2D**

The dynamic time courses of cytoskeletal remodeling are consistent in many ways with observations of cytoskeletal dynamics in 2D and with our earlier quasi-static observations of cell dynamics in 3D, but differ in several important ways as well. Post-stretch fluidization is consistent with the Fredberg model (Deng, Trepap et al. 2006) of cytoskeletal fluidization induced exclusively through mechanical means. The general picture of actin stress fiber depolymerization followed by repolymerization into the direction of principal straining is consistent with the 2D Deshpande model (Deshpande, McMeeking et al. 2006) of staged actin stress fiber dynamics relating to a preferred stress range.

Contrary to observations of cells in 2D, retraction and reinforcement responses could both be observed at sustained nominal stretches, and occurred independently of cell orientation, cell morphology, and peak principal strain. This diversity of responses can be attributable to local mechanical conditions, beyond the resolution of our strain measurements, to ETC-level mechanical structures that transmitted stresses preferentially to some cells, or to diversity in the mechanical and biochemical life

histories of individual cells. Results could also be rectified with the 2D Fredberg and Deshpande models of cytoskeletal behavior if, as is fully possible in 3D, the local mechanical environment changed significantly over the course of several minutes, either due to cellular or ECM changes. Assessing these possibilities in an ETC will require additional development of experimental techniques.

Additional distinctions between cytoskeletons in 2D and our observations of cells in 3D ETCs were the absence of lamellipodia and the presence of patches of F-actin. Although lamellipodia did not appear in any of the many hundreds of cells we observed in 3D ETCs, observations of lamellipodia dynamics may shed some light on the role and function of the F-actin patches. Lamellipodia are relatively stiff networks of F-actin (Felder and Elson 1990), and the F-actin in these networks exhibits retraction to rounded masses in neurons cultured in 2D and treated with cytochalasin B (Forscher and Smith 1988), possibly due to contractile tension in the fibers (Verkhovskiy, Svitkina et al. 1999). In 3D ETCs, F-actin patches appeared at times when other cytoskeletal features such as stress fibers and filopodium-like extensions disappeared, and disappeared when these other features reappeared, suggesting that they might serve as reservoirs, or might in fact be related to stress fibers that have retracted.

While the local environment of a contractile fibroblast surrounded by collagen in an ETC differs so fundamentally from that of a cell in 2D culture that focal attachments and filopodia are difficult to relate, some consistencies should be noted. Filopodia-like extensions occurred in the direction of ETC stretch and under conditions

associated with development of stress fibers, consistent with observations that cellular contraction is associated with filopodia extension in 2D (Grinnell 1994). The extension of filopodia into the direction of principal stretch and the alignment of stress fibers in this direction is consistent with the wealth of experimental data and biophysical models that predict such polarity of endothelial cells subjected to very low frequency stretch (Hsu, Lee et al. 2009; Hsu, Lee et al. 2010) (Lee, Haase et al. 2010); (De and Safran 2008; De, Zemel et al. 2010); (Zemel and Safran 2007; Zemel, Rehfeldt et al. 2010; Zemel, Rehfeldt et al. 2010).

While data on cellular dynamics in 3D culture are much more sparse, our data show some consistencies and new perspectives. The general picture of cells elongating into the direction of mechanical constraint has long been known (Grinnell 1994), and our data show that this occurs following stretch. Our data also suggest that a diversity of cell shapes can exist throughout an ETC, suggesting once more ETC-level structures of cellular and mechanical connectivity that are important to the cellular mechanical environment. Our previous studies showed that, under isometric conditions following a rapidly applied stretch, the actin cytoskeletons of contractile fibroblasts within ETCs depolymerized initially then returned to approximately the same or a slightly higher density of actin stress fibers (Nekouzadeh, Pryse et al. 2008). However, the key difference with the present study is that only a fraction of cells in each image expressed fluorophors, and a diversity of responses were observed. Retraction responses in some cells might be countered by reinforcement responses in neighboring cells. Taken in

combination with these earlier results, the present results suggest the possibility of a homeostasis at the level of the entire ETC that can be achieved by individual cells.

### **2.4.3 Stress Fiber Formation Does Not Require the Rho Pathway**

The GTPase rhoA influences many aspects of cell shape and motility through regulation of actin stress fiber formation and activation of rho kinase (ROCK) to promote actin-myosin II contraction (Olson 2008). Y-27632 inhibits ROCK and therefore interferes with the RhoA/ROCK pathway and stress fiber contraction. Although ROCK inhibition results in actin cytoskeleton reorganization and morphological changes in cells cultured in 2D, Y-27632 was not observed to significantly alter cell morphology in ETCs, and did not affect mechanically-induced stress fiber formation. ROCK regulates actin-myosin II interaction by phosphorylation in two ways: through the myosin-binding subunit (MBS) of myosin light chain phosphatase and through myosin regulatory light chain (MRLC) in the absence of  $Ca^{2+}$  (Kimura, Ito et al. 1996). This appeared to occur in the 3D ETCs, because ROCK inhibition did decrease contractile force (Supplemental Results, section SR-4).

In addition to ROCK, myosin light chain kinase (MLCK), a  $Ca^{2+}$ /calmodulin-dependent enzyme, regulates the assembly of stress fibers and focal adhesions in fibroblasts cultured in 2D (Burrige and Chrzanowska-Wodnicka 1996; Totsukawa, Yamakita et al. 2000; Katoh, Kano et al. 2001). MLCK also regulates contractility in

non-muscle cells by phosphorylating the myosin regulatory light chain in a  $\text{Ca}^{2+}$ -dependent way (Katoh, Kano et al. 2001). In ETCs, depletion of intracellular or extracellular  $\text{Ca}^{2+}$  did not show a relaxation of intracellular stresses (that is, no elongation in the direction of isometric ETC stretch or retraction perpendicular to this direction), indicating that the MLCK pathway was not a significant contributor to cellular contraction. However, results support the idea that the MLCK-pathway rather than the rho pathway is important for mechanical induction of actin stress fibers.

#### **2.4.4 Limitations**

Finally, we note several aspects of our method that must be considered when interpreting data. The first is Poisson contraction of stretched, ring-like ETCs, which could allow ETCs to move a small distance from the objective, altering intensities and sizes measured for fluorescent beads or transfected cells. However, control studies in which ETCs were lifted from the microscope objective by a glass slide did not show appreciable effects. The second is dynamic activity of cells within ETCs, which can continue to remodel themselves and the ECM and thereby move out-of-focus. This forced some data to be discarded.

The third aspect of is the anisotropic and nonuniform nature of the ETCs. The ETCs are anisotropic, with a preferred circumferential direction for collagen fibers. Since ETCs are therefore stiffer in the imaging region, where stretch aligns with the circumferential direction of the ETC, than in the region contacting the loading bars, where stretch is in the radial direction of the ETC, we expect the nonuniform strain

field (cf. (Thomopoulos, Das et al. 2011)), with the result that strain in the imaging region is smaller than the nominal strain between the loading bars. To establish relationship between strain at the loading bars and strain within the specimen, strains were estimated over the region of the tissue construct in which cells were imaged using standard protocols involving tracking of fluorescent beads (Legant, Miller et al. 2010). The strain parallel to the stretch direction was approximately 5.6% following a 10% stretch of the ETC, and 9.7% following a 30% stretch of the ETC (Supplemental Results, Fig. S7-1). Transverse contraction was approximately 5.2% following the 10% stretch and ~11% following the 30% stretch. This indicated that the tissue constructs were highly anisotropic. Tissue constructs are also nonuniform due to variations in ECM remodeling by cells. While these complicate interpretation of data, these might also be important features of cells in living tissues.

The final aspect that needs careful consideration is the interpretation of quantitative stereologic measures. The first metric applied was area projected cell area, which proved a sensitive measure for physical changes to cells for the specific conditions in the ETCs tested; however, this might not be the case for other ETCs. With the cell density in the ETCs above the percolation threshold, cells and ECM are expected to deform in registry (Marquez, Genin et al. 2005; Marquez, Genin et al. 2005). Because the tissue constructs were so highly anisotropic (Poisson's ratio relating circumferential stretch to lateral contraction close to 1), expected area changes due to passive stretch were very small, and measured area changes could be attributed to active cellular processes such as polymerization and depolymerization of actin stress fibers,

and detachment from the ECM (Supplemental Discussion, section SD-3). Polymerization of actin stress fibers and detachment from the ECM decreased area, and depolymerization, which would be expected to make the actin cytoskeleton more compliant, increased areas. The role of active stresses in these reductions was evident in the rate at which area reduced to approximately pre-stretch levels, with recovery occurring faster at the lower stretch magnitude. The measured increases of cell area, especially following higher stretch, were consistent with a reduction of cell stiffness associated with fluidization (Marquez, Elson et al. 2010).

The cell perimeter was more difficult to interpret, because it included contributions from extension and retraction of filopodia, which could balance out one another. However, changes to the fibrosity measure proved sensitive to the polymerization and depolymerization of stress fibers, especially when combined with area. In combination, these metrics enabled observations supporting our hypotheses that individual contractile fibroblast cells in ETCs would respond to mechanical stretches through remodeling at the cellular and cytoskeletal levels. Results showed that the apparent mechanism for this involves an interplay with F-actin patches, and that interesting and fundamentally different behaviors can be observed by exploring cellular dynamics in a 3D environment.



## 2.5 Supplemental Document

### 2.5.1 Supplemental Methods

#### 2.5.1.A SM-1. Strain Estimation

To evaluate passive deformation in the imaged regions of the ETCs, fluorescent beads were added to some ETCs and their displacements were tracked the reference subset image (before stretch) to the deformed subset image (after mechanical stretch). Approximate strains were computed by least squares linear fitting over a rectangular region. Briefly, normalized bead positions and displacements in the in-plane ( $x$  and  $y$ ) directions of a collapsed confocal stack of images were estimated for each tracked bead  $k$ :  $\bar{\mathbf{u}}^{(k)} = u_x^{(k)} \hat{\mathbf{i}} + u_y^{(k)} \hat{\mathbf{j}}$ , where  $-1 \leq x \leq 1$  and  $-1 \leq y \leq 1$  are Cartesian coordinates normalized so that all tracked beads fall into a unit square, and  $\hat{\mathbf{i}}$  and  $\hat{\mathbf{j}}$  are associated unit vectors. Then, the displacement field  $u_x(x, y)$  and  $u_y(x, y)$  can be expressed in the form  $u_i(x, y) = \sum_{k=1}^4 N_k(x, y) U_{k_i}$ , where  $i = x, y$ ,  $N$  is a standard first order shape function (e.g. Bower, 2010) and  $U$  is the normalized displacement of one of the four corner nodes of the region. The deformation gradient tensor,  $\mathbf{F}_{ij} = \delta_{ij} + \frac{\partial u_i}{\partial x_j}$ , in which  $\delta_{ij}$  is Kronecker's delta function, can be calculated from the interpolated strain field. From this the Green-Lagrange strain tensor,  $\mathbf{E}_{ij} = \frac{1}{2}(\mathbf{F}_{ki} \mathbf{F}_{kj} - \delta_{ij})$ , where repeated indices imply summation, was calculated.

## 2.5.2 Supplemental Results

### 2.5.2.A SR-1. Stress fibers and actin patches contain organized $\alpha$ -actinin

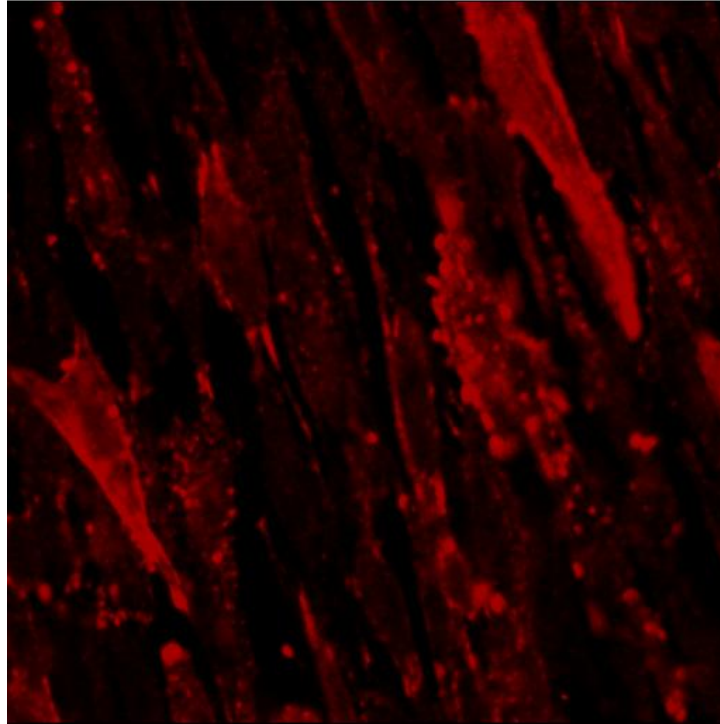


**Figure SR- 1  $\alpha$ -actinin staining cells in the ETC**

Stress fibers and actin patches observed in cells within ETCs displayed organized but poorly striated distributions of  $\alpha$ -actinin (red stain). Following preconditioning and a mechanical stretch of 10%, ETCs were fixed in their stretched state using 4% paraformaldehyde, then stained with both primary and secondary antibodies using standard procedures to reveal  $\alpha$ -actinin.

### 2.5.2.B SR-2. ETCs Responded Viscoelastically and Actively to Mechanical Stretch

Following mechanical stretch, the isometric force needed to sustain a specimen at prescribed length increased above its baseline level, then decreased to slightly above

the baseline pre-stretch value over the course of approximately 30 minutes, as the ECM and cells relaxed viscoelastically and as the cells remodeled actively.

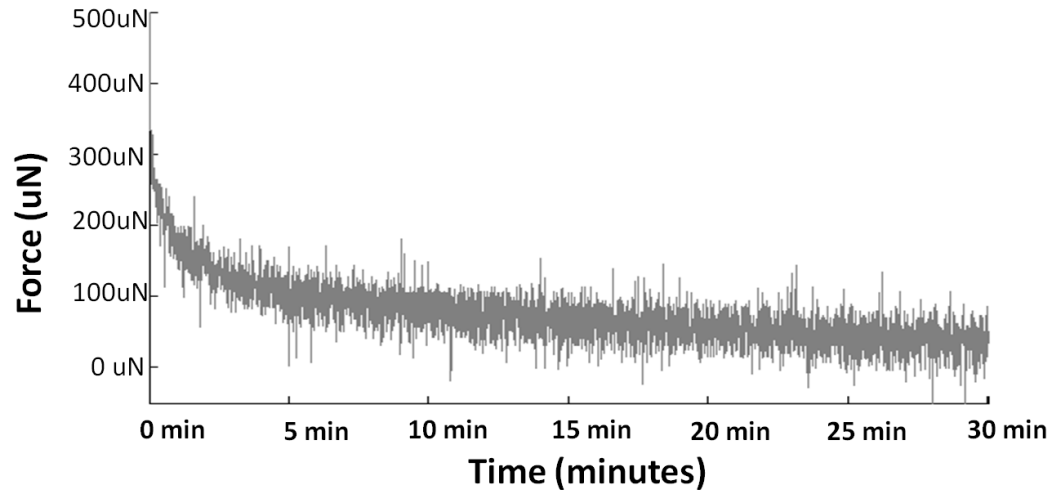


**Figure SR- 2 Typical curve of force relaxation**

Force data was recorded simultaneously while the ETC was subjected to the mechanical stretch. This figure showed a typical force relaxation process of the ETC in response to the mechanical stretch. The time duration in our experiment was 30 minutes while the ETC was stretched and held. While the high frequency oscillations were due to noise, the lower frequency oscillations were attributable to active cellular contractions and do not appear in relaxation curves associated with passive materials.

### 2.5.2.C SR-3. Stellate and Spindle Cells Both Reinforced Their Cytoskeletons in the Direction of Mechanical Stimulus

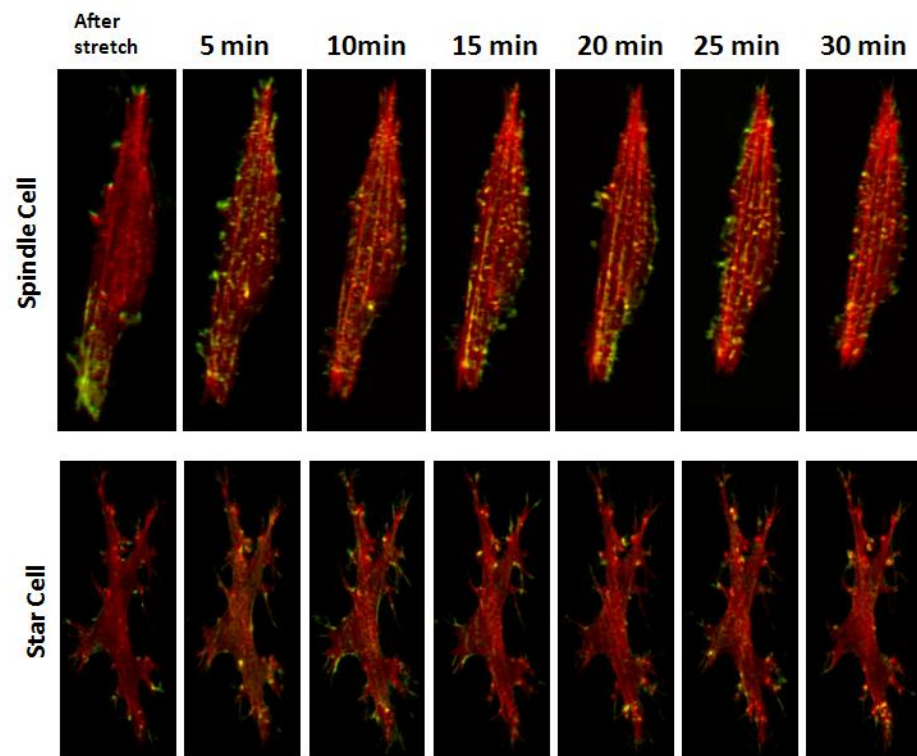


**Figure SR- 3 Time variation of cytoskeleton in stellate and spindle cells. Time course of changes to the actin cytoskeletons of two cells.**

Frame-to-frame differences (green) in the actin cytoskeletons (red) both showed reinforcement in the direction of mechanical stretch (vertical) during to an isometric hold while cells were stretched 10%. The spindle cell generated new stress fibers or modulated actin patches as it shrank. Growth and remodeling of stress fibers was also observed in the stellate cell. The majority of stretch-induced remodeling paralleled the direction of mechanical stretch. Sparse actin patches near sites of cytoskeletal remodeling were also observed in stellate cells after stretch. These data support the conclusion that contractile fibroblasts in an

ETC actively contracted and remodeled in response to alterations in their mechanical environments, independent of cell morphology.

#### 2.5.2.4 SR-4. Effects of Y-27632 on Cellular Morphology and Mechanics

Cell morphology and mechanics were assayed in ETCs treated with 10  $\mu\text{M}$  Y-27632 that were stretched by 10% and 30% and then held isometrically. Results indicate that generation of stress fibers and cytoskeletal reinforcement do not require the rho kinase pathway (Fig. SR-4), and that significant morphological changes can occur in the absence of this pathway (Fig. SR-5). Further, the active contractile force associated with Y-27632 was independent of the degree to which the ETC was stretched (Fig. SR-6).

This latter result indicates that the average contractile force per cell was the same in ETCs stretched to different degrees. The following simple estimate suggests that the average force per unit area was close as well, and lends support to the contention that the transfected cells behaved much like their wild type counterparts because the magnitude of contractile stress found was close to that reported for wild type cells. Approximating a cell ECM as transversely isotropic, defining the stretch ratio in the direction of ETC stretch as  $\lambda_P$  and the stretch ratio in all directions perpendicular to this as  $\lambda_T$ , and approximating the cell as incompressible, the relation  $\lambda_P \lambda_T^2 = 1$  holds. Then, the active contractile Cauchy stress can be written as a function of the active contractile force  $F(\lambda_P)$  and the initial cross-sectional area  $A_0$  as  $\sigma_0 = F/(\lambda_T^2)A_0 = \lambda_P F/A_0$ . The initial cross-sectional area of the ETCs was measured using confocal microscopy as  $A_0 \approx 9.66 \times 10^{-7} \text{ m}^2$ . Although the strain field in

the ETCs was certainly non-uniform, an estimate of the mean active stresses can still be estimated from these formulae. The appropriate stretch ratio to use is the stretch ratio measured within specimen rather than the nominal ETC stretch ratio. For the 10% and 30% stretches, these were  $\lambda_{10\%} = 1.056$  and  $\lambda_{30\%} = 1.097$ . Plugging in,  $\sigma_o^{10\%} \approx 116$  Pa, and  $\sigma_o^{30\%} \approx 119$  Pa.

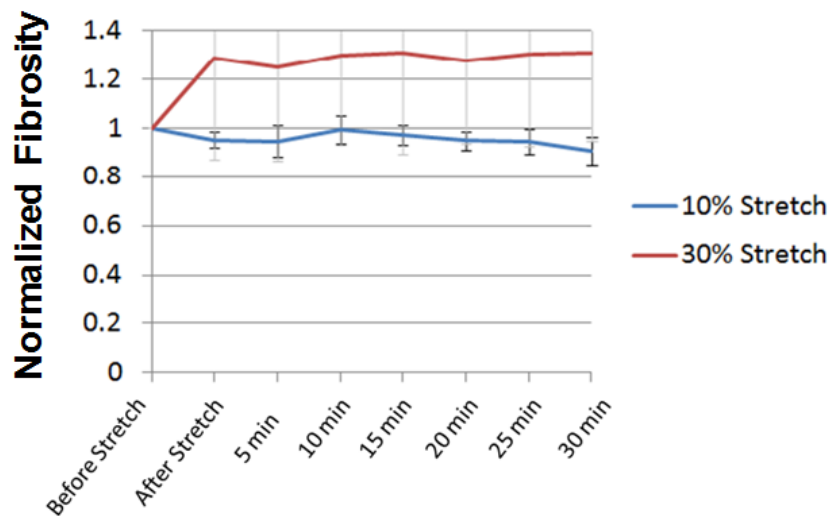


**Figure SR- 4 Time course of fibrosity treated with Y-27632**

Time course of fibrosity during experiments in which ETCs treated with 10  $\mu$ M Y-27632 were stretched by 10% and 30% and then held isometrically. The fibrosity was largely unaffected by the smaller amplitude stretch, but increased significantly following the larger amplitude stretch. This latter rise was associated with the formation of stress fibers (Supplemental Movie 5). Results indicate that generation of stress fibers and cytoskeletal reinforcement do not require the rho kinase pathway.

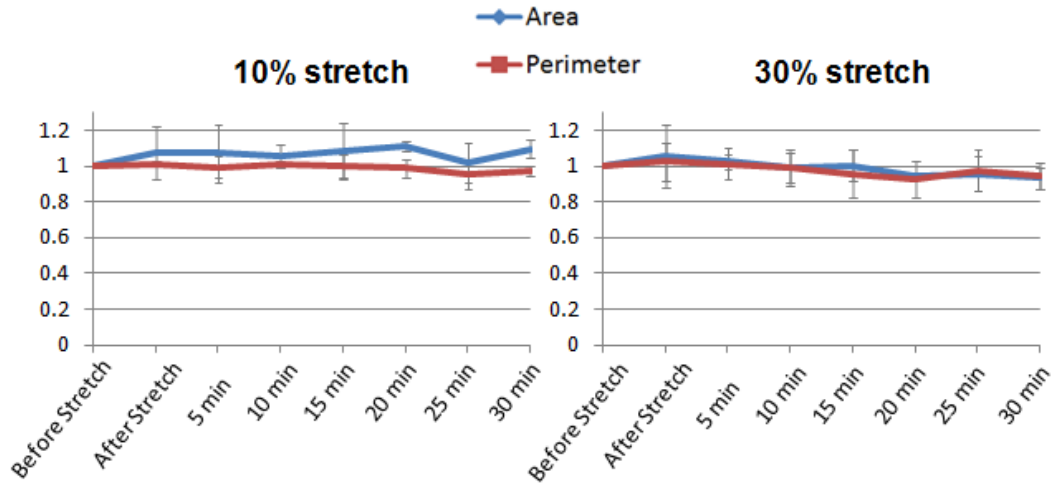


**Figure SR- 5** Time course of cellular area and perimeter treated with Y-27632

Time course of cellular area and perimeter in cells (n=3) during experiments in which ETCs treated with Y-27632 were stretched by 10% and 30% and then held isometrically. Area increased in these cells following 10% stretch, but decreased following 30% stretch. Blocking the rho kinase pathway using Y-27632 therefore does not eliminate the ability of these cells to alter their morphology.

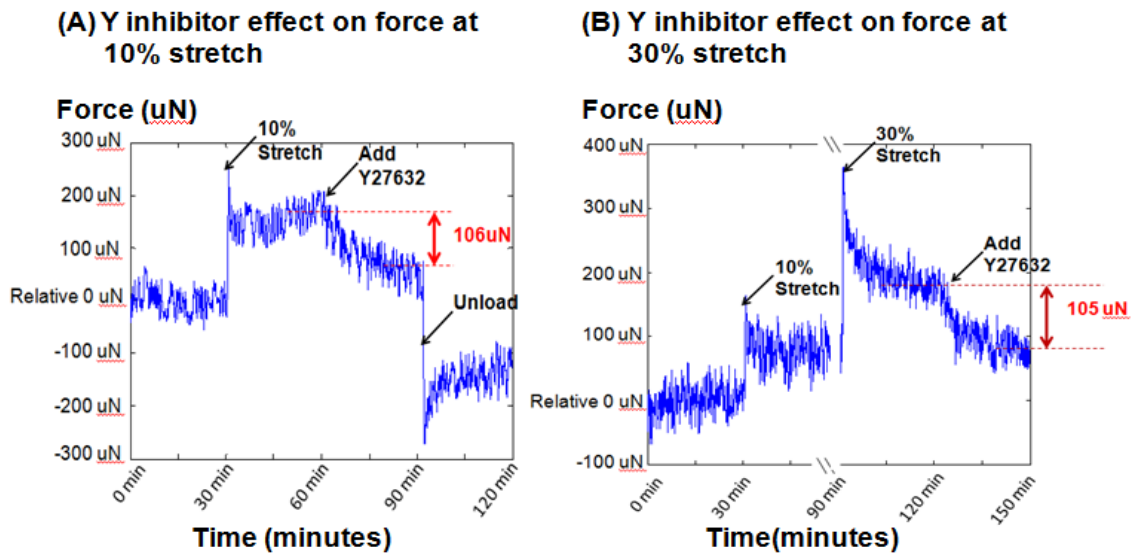


**Figure SR- 6 Force response of cells treated with Y-27632 at different stretch level**

Effects of Y-27632 on force responses of an ETC stretched 10% (A) and of a different ETC first stretched 10%, and then stretched 30%; in both cases, the preconditioning and relaxation protocols described in Methods were followed. The reductions in active contractile forces (and, as described in the text of this section (SR-4), the active contractile stresses) associated with the addition of Y-27632 was independent of the level of stretch: 106  $\mu\text{N}$  following 10% stretch, and 105  $\mu\text{N}$  following 30% stretch. These observations support those of Wakatsuki et al. (2000) that cellular contractile forces are independent of the degree to which cells are stretched in a 3D ETC.



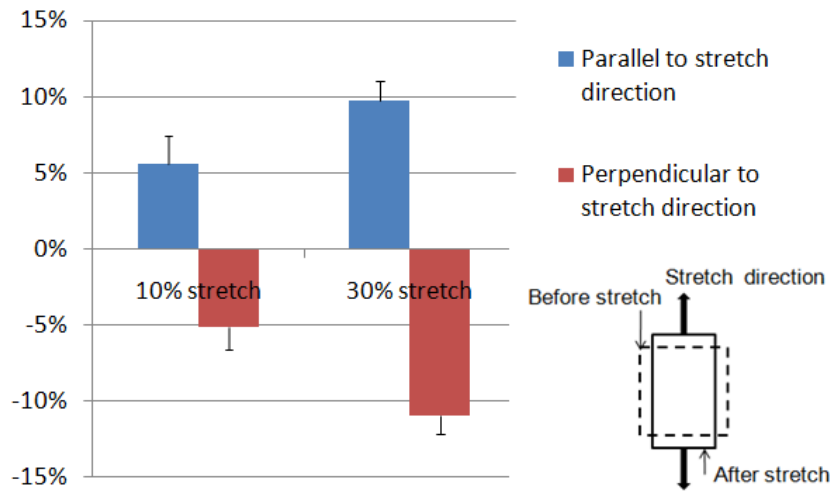


**Figure SR- 7 Local strains as a function of the nominal strains on the ETC.**

The methods of section SM-1 were used to estimate the strain in the ETCs after the mechanical stretch. Comparing to 10% stretch, 30% stretch produced longer elongation parallel to the stretch direction (5.6% to 10%) and shrank in the direction perpendicular to the stretch (5.2% to 10.9%). The effective Poisson ratio of  $\sim 1$  is within the thermodynamic bounds for a transversely isotropic material.

## 2.5.3 Supplemental Discussion

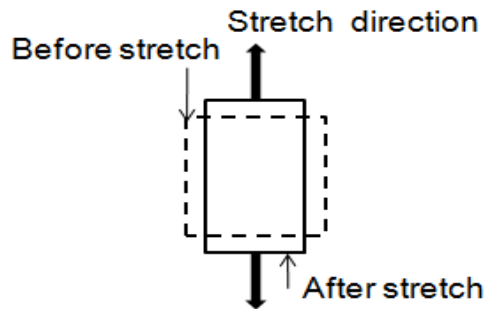
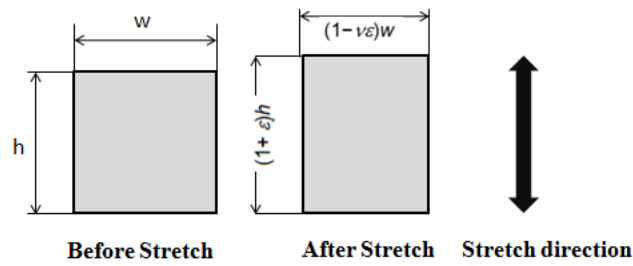
### 2.5.3.A SD-1. Relationship between Cell locomotion and Cellular Remodeling

Many but not all fibroblasts developed visible stress fibers in response to mechanical cues. While cells continuously alter their morphology without the mechanical cues, changes following mechanical cues follow one of three patterns.

Actin in cells is dynamic and undergoes a cycle of polymerization and depolymerization. Alterations to this cycle enable the actin cytoskeleton to respond to the external stimuli from the cellular micro-environment. Actin assembly in eukaryotic cell motility is widely thought to drive protrusion at the leading edge of the cell (Pantaloni, Le Clainche et al. 2001; Mogilner and Oster 2003; Pollard and Borisy 2003). Emerging evidence suggests that stress fiber formation and contractility are important in tail retraction (Pellegrin and Mellor 2007).

Cell migration is recognized as a cyclic process of protrusion, traction and retraction. During cell locomotion, forces developed in the actin microfilament system are believed to be transmitted to the substrate to drive protrusion at the leading edge of the cell. In ETCs, obvious cell migration was not noticeable. Before stretch, cells extended and retracted protrusions without preference to orientation. After stretch, cells tended to retract protrusions perpendicular to the stretch direction and extend them along the stretch direction; however, these extensions and retractions did not move the cells' centers of mass appreciably.

### 2.5.3.B SD-2. Effects of Passive Stretch on Area and Perimeter



To estimate the degree to which cells responded actively to mechanical stretch, a simple example was studied that elucidated expected changes in area and perimeter for alterations to cell morphology. This model was predicated on the observation of Marquez et al. (2010) that contractile fibroblasts and ECM have approximately the same elastic moduli in ETCs under the conditions tested, in which ETCs contain a population of cells just above the percolation threshold. In this case, the strain in the local ECM should approximately equal that in the cells. For the idealized “cell” in the above figure of width  $w$  and height  $h$ , the initial area can be estimated by assuming the area associated with filopodia-like extensions to be small as  $A_0 = wh$ . Following stretch to a nominal strain  $\epsilon$ , the cell’s height grows to  $(1 + \epsilon)h$  and its width shrinks to approximately  $(1 - \epsilon\nu_{LT})w$ , where the Poisson ratio  $\nu_{LT}$  relating transverse constriction to longitudinal extension of the area element was measured to be on the order of 0.9 to 1.1. Then, the ratio of final to initial area is:

$$\frac{A}{A_0} = \mathbf{1} + (\mathbf{1} - \nu_{LT})\epsilon - \nu_{LT}\epsilon^2.$$

For the strain range studied in this work, this yields estimates of  $A/A_0$  between 0.98 and 1.00 for passive changes to cell area. Therefore, any significant deviations of area are indicative of active cellular remodeling.

Measurement of cell perimeter are more difficult to interpret because these must include the contributions of filopodia-like extensions. The perimeter measurement algorithm used counts both sides of each filopodium, so the initial perimeter as reported through the algorithm used is  $p_0 \approx 2(w + h + L_f)$ , where  $L_f$  is the total pre-stretch length of all filopodia. Following stretch, the final perimeter is approximately:

$$p \approx 2\left((\mathbf{1} - \nu_{LT}\epsilon)w + (\mathbf{1} + \epsilon)h + L_f\right),$$

where  $L_f$  is the total post-stretch length of all filopodia. For a spindle-shaped cell,  $h \gg w$  and few filopodia are observed ( $L_f \approx 0$ ), and

$$\frac{p}{p_0} \approx (\mathbf{1} + \epsilon).$$

For a stellate cell,  $h \approx w$ , and the directions of filopodia are important. Then, following stretch,

$$\frac{p}{p_0} = \frac{2\left((\mathbf{1} - \nu_{LT}\epsilon)w + (\mathbf{1} + \epsilon)h + L_f\right)}{2(w + h + L_f)} \sim \frac{2 + (\mathbf{1} - \nu_{LT})\epsilon + L_f/h}{2 + L_f/h} \sim \frac{2 + L_f/h}{2 + L_f/h}$$

where the last step is true for  $\nu_{LT}$  close to 1. The perimeter measurements therefore represent predominantly changes in filopodial lengths in stellate cells. However, these are difficult to interpret in the context of cellular responses to stretch, because our

observations suggested reduction in length in the transverse direction associated with extension in the axial direction. Therefore, for both stellate and spindle-shaped cells, perimeter measurements proved less informative than area measurements for understanding temporal changes to cellular morphology.

## 2.7 References:

- Bayly, P. V., K. T. Dikranian, et al. (2006). "Spatiotemporal evolution of apoptotic neurodegeneration following traumatic injury to the developing rat brain." Brain Res 1107(1): 70-81.
- Burridge, K. and M. Chrzanowska-Wodnicka (1996). "Focal adhesions, contractility, and signaling." Annu Rev Cell Dev Biol 12: 463-518.
- De, R. and S. A. Safran (2008). "Dynamical theory of active cellular response to external stress." Phys Rev E Stat Nonlin Soft Matter Phys 78(3 Pt 1): 031923.
- De, R., A. Zemel, et al. (2010). "Theoretical concepts and models of cellular mechanosensing." Methods Cell Biol 98: 143-175.
- Deng, L., X. Trepap, et al. (2006). "Fast and slow dynamics of the cytoskeleton." Nat Mater 5(8): 636-640.
- Deshpande, V. S., R. M. McMeeking, et al. (2006). "A bio-chemo-mechanical model for cell contractility." Proc Natl Acad Sci U S A 103(38): 14015-14020.
- Felder, S. and E. L. Elson (1990). "Mechanics of fibroblast locomotion: quantitative analysis of forces and motions at the leading lamellas of fibroblasts." J Cell Biol 111(6 Pt 1): 2513-2526.
- Forscher, P. and S. J. Smith (1988). "Actions of cytochalasins on the organization of actin filaments and microtubules in a neuronal growth cone." J Cell Biol 107(4): 1505-1516.
- Forte, A., A. Della Corte, et al. (2010). "Role of myofibroblasts in vascular remodelling: focus on restenosis and aneurysm." Cardiovasc Res 88(3): 395-405.
- Fredberg, J. J. (2002). "Airway narrowing in asthma: does speed kill?" Am J Physiol Lung Cell Mol Physiol 283(6): L1179-1180.
- Friedl, P. and E. B. Brocker (2000). "The biology of cell locomotion within three-dimensional extracellular matrix." Cell Mol Life Sci 57(1): 41-64.
- Geiger, B., A. Bershadsky, et al. (2001). "Transmembrane crosstalk between the extracellular matrix--cytoskeleton crosstalk." Nat Rev Mol Cell Biol 2(11): 793-805.
- Grinnell, F. (1994). "Fibroblasts, myofibroblasts, and wound contraction." J Cell Biol 124(4): 401-404.
- Hsu, H. J., C. F. Lee, et al. (2009). "A dynamic stochastic model of frequency-dependent stress fiber alignment induced by cyclic stretch." PLoS One 4(3): e4853.
- Hsu, H. J., C. F. Lee, et al. (2010). "Stretch-induced stress fiber remodeling and the activations of JNK and ERK depend on mechanical strain rate, but not FAK." PLoS One 5(8): e12470.
- Katoh, K., Y. Kano, et al. (2001). "Rho-kinase--mediated contraction of isolated stress fibers." J Cell Biol 153(3): 569-584.
- Kaunas, R. and H. J. Hsu (2009). "A kinematic model of stretch-induced stress fiber turnover and reorientation." J Theor Biol 257(2): 320-330.
- Kaunas, R., S. Usami, et al. (2006). "Regulation of stretch-induced JNK activation by stress fiber orientation." Cell Signal 18(11): 1924-1931.

- Kimura, K., M. Ito, et al. (1996). "Regulation of myosin phosphatase by Rho and Rho-associated kinase (Rho-kinase)." Science 273(5272): 245-248.
- Krishnan, R., C. Y. Park, et al. (2009). "Reinforcement versus fluidization in cytoskeletal mechanoresponsiveness." PLoS One 4(5): e5486.
- Lee, C. F., C. Haase, et al. (2010). "Cyclic stretch-induced stress fiber dynamics - dependence on strain rate, Rho-kinase and MLCK." Biochem Biophys Res Commun 401(3): 344-349.
- Legant, W. R., J. S. Miller, et al. (2010). "Measurement of mechanical tractions exerted by cells in three-dimensional matrices." Nat Methods 7(12): 969-971.
- Marquez, J. P., E. L. Elson, et al. (2010). "Whole cell mechanics of contractile fibroblasts: relations between effective cellular and extracellular matrix moduli." Philos Transact A Math Phys Eng Sci 368(1912): 635-654.
- Marquez, J. P., G. M. Genin, et al. (2006). "Cellular and matrix contributions to tissue construct stiffness increase with cellular concentration." Ann Biomed Eng 34(9): 1475-1482.
- Marquez, J. P., G. M. Genin, et al. (2005). "The relationship between cell and tissue strain in three-dimensional bio-artificial tissues." Biophys J 88(2): 778-789.
- Marquez, J. P., G. M. Genin, et al. (2005). "Thin bio-artificial tissues in plane stress: the relationship between cell and tissue strain, and an improved constitutive model." Biophys J 88(2): 765-777.
- McGarry, J. P. (2009). "Characterization of cell mechanical properties by computational modeling of parallel plate compression." Ann Biomed Eng 37(11): 2317-2325.
- Mogilner, A. and G. Oster (2003). "Force generation by actin polymerization II: the elastic ratchet and tethered filaments." Biophys J 84(3): 1591-1605.
- Nekouzadeh, A., K. M. Pryse, et al. (2008). "Stretch-activated force shedding, force recovery, and cytoskeletal remodeling in contractile fibroblasts." J Biomech 41(14): 2964-2971.
- Olson, M. F. (2008). "Applications for ROCK kinase inhibition." Curr Opin Cell Biol 20(2): 242-248.
- Pantaloni, D., C. Le Clairche, et al. (2001). "Mechanism of actin-based motility." Science 292(5521): 1502-1506.
- Pellegrin, S. and H. Mellor (2007). "Actin stress fibres." J Cell Sci 120(Pt 20): 3491-3499.
- Pollard, T. D. and G. G. Borisy (2003). "Cellular motility driven by assembly and disassembly of actin filaments." Cell 112(4): 453-465.
- Rohr, S. (2009). "Myofibroblasts in diseased hearts: new players in cardiac arrhythmias?" Heart Rhythm 6(6): 848-856.
- Small, J. V., K. Rottner, et al. (1998). "Assembling an actin cytoskeleton for cell attachment and movement." Biochim Biophys Acta 1404(3): 271-281.
- Taber, L. A. (2009). "Towards a unified theory for morphomechanics." Philos Transact A Math Phys Eng Sci 367(1902): 3555-3583.
- Thastrup, O., P. J. Cullen, et al. (1990). "Thapsigargin, a tumor promoter, discharges intracellular Ca<sup>2+</sup> stores by specific inhibition of the endoplasmic reticulum Ca<sup>2+</sup>(+)-ATPase." Proc Natl Acad Sci U S A 87(7): 2466-2470.
- Thomopoulos, S., R. Das, et al. (2011). "Fibrocarrilage tissue engineering: the role of the stress environment on cell morphology and matrix expression." Tissue Eng Part A 17(7-8): 1039-1053.

- Thomopoulos, S., G. R. Williams, et al. (2003). "Tendon to bone healing: differences in biomechanical, structural, and compositional properties due to a range of activity levels." J Biomech Eng 125(1): 106-113.
- Totsukawa, G., Y. Yamakita, et al. (2000). "Distinct roles of ROCK (Rho-kinase) and MLCK in spatial regulation of MLC phosphorylation for assembly of stress fibers and focal adhesions in 3T3 fibroblasts." J Cell Biol 150(4): 797-806.
- Trepat, X., L. Deng, et al. (2007). "Universal physical responses to stretch in the living cell." Nature 447(7144): 592-595.
- Verkhovsky, A. B., T. M. Svitkina, et al. (1999). "Network contraction model for cell translocation and retrograde flow." Biochem Soc Symp 65: 207-222.
- Vogel, V. and M. Sheetz (2006). "Local force and geometry sensing regulate cell functions." Nat Rev Mol Cell Biol 7(4): 265-275.
- Wakatsuki, T., M. S. Kolodney, et al. (2000). "Cell mechanics studied by a reconstituted model tissue." Biophys J 79(5): 2353-2368.
- Zemel, A., F. Rehfeldt, et al. (2010). "Cell shape, spreading symmetry and the polarization of stress-fibers in cells." J Phys Condens Matter 22(19): 194110.
- Zemel, A., F. Rehfeldt, et al. (2010). "Optimal matrix rigidity for stress fiber polarization in stem cells." Nat Phys 6(6): 468-473.
- Zemel, A. and S. A. Safran (2007). "Active self-polarization of contractile cells in asymmetrically shaped domains." Phys Rev E Stat Nonlin Soft Matter Phys 76(2 Pt 1): 021905.



# Chapter 3 : Dynamics of Membrane Retraction in a Three Dimensional Tissue Construct

In traditional tissue culture systems, cells are grown on two-dimensional (2D) solid surfaces. However, increasing evidence indicates that cells in three-dimensional (3D) systems may have different adhesion, morphology, and biological responses to biophysical factors. A 3D culture system therefore may be a more appropriate model system that mimics native cell environments and thereby allows controlled exploration of cell functions and responses. Through study of engineered tissue construct (ETCs) in a specialized testing system, we integrated both a programmable mechanical stretching device and confocal fluorescence microscopy to explore whole cell behaviors of contractile fibroblast cells in a 3D environment. From a series of tests, we found that shapes of stained cells, defined by the outline of their lipid membranes, are more star-like (“stellate”) when cultured in a low cell concentration. In a high cell concentration, cells are more spindle-like. When ETCs are stretched and then held isometrically, stellate cells extend processes in the direction of stretch and release processes in the directions perpendicular to stretch. However, under the same stretching protocol, some spindle cells detach from the extracellular matrix (ECM), then retract. Misaligned spindles extend processes primarily but not exclusively in the direction of stretch. Furthermore, measurements of time constants among groups with different mechanical cues show two results. The first is that the propensity of cell processes to retract

decreases with increasing stretch of the tissue construct. The second is that mechanical preconditioning modulates the way that cells respond to their environment. These studies indicate that cells in a 3D environment respond actively to external mechanical stimuli, and have implications for the role of mechanical stretch in wound healing scenarios.

### **3.1 Introduction**

The cell membrane, consisting of a phospholipid bilayer with embedded proteins, is a biological interface that separates the intracellular from the extracellular environment. A variety of cellular processes such as cell adhesion, cell signaling and ion conductivity are involved in the communication across the cell membrane. These interactions between cells and their environments produce a series of physiological responses including polarization, protrusion, adhesion, signal regulation and integration. These responses are important in embryonic development, wound healing, inflammatory process and disease.

Fibroblasts are responsible for collagen biosynthesis and organization in connective tissues, and play a role in regulation of epithelial differentiation, regulation of inflammation, and wound healing. Increasing evidence suggests that some fibroblasts might promote tumors by facilitating angiogenesis and cancer progression (Kalluri and Zeisberg 2006). Fibroblasts are mechanically coupled to their fibrillar ECM, which can regulate cell behavior through its composition and mechanics. Therefore, the study of

fibroblasts in three dimensional (3D) tissues would help investigate cell responses normally occurring *in vivo*.

The goal of this work was to establish a platform to quantify the membrane responses of fibroblasts in the engineered tissue constructs (ETCs) in response to external mechanical stimuli. ETCs were stretched, and then held isometrically while morphology was tracked by confocal fluorescence microscopy and isometric force was monitored.

Results are of interest in two contexts. The first is in relation to cytoskeletal responses observed in Chapter 2. To what degree do the time constants associated with F-actin remodeling within the cytoskeleton differ from those associated with membrane remodeling? We hypothesized that these time constants are independent of degree of stretch, and are statistically indistinguishable from those associated with cytoskeletal remodeling. Results supported this hypothesis. The second is in relation to mathematical models of living cells. To what degree do time constants associated with membrane remodeling differ from those of membrane tether retraction, for instance in pure lipid membrane tethers associated with leukocyte rolling (e.g. (Girdhar and Shao 2004; Chen, Girdhar et al. 2007; Girdhar and Shao 2007; Liu, Goergen et al. 2007; Yu and Shao 2007; Chen, Yao et al. 2010))? We hypothesized that factors such as membrane structures and cytoplasmic poroelasticity would retard retraction rates relative to those of pure membrane, and results supported this hypothesis.

## 3.2 Materials and Methods

### 3.2.1 Preparation of Engineered 3D Tissue Constructs

Chicken embryo fibroblast (CEF)-populated collagen gel ETCs were made following the protocol reported by others (Wakatsuki, Kolodney et al. 2000), with two exceptions. First, the membranes of a fraction of cells were stained with a fluorescent membrane dye as described below. Second, fluorescent microspheres were added in prescribed quantities to a fraction of ETCs. Briefly, CEFs isolated from 10-day chicken embryos (Fertile White Leghorn Chicken Eggs, Sunrise Farms, Catskill, NY) were maintained in Dulbecco's modified Eagle's medium (DMEM) with 10% fetal calf serum (FCS), penicillin and streptomycin at 50 units/ml and 50  $\mu\text{g}/\text{ml}$  respectively but without phenol red, a pH indicator. The CEFs in 10% FCS DMEM were then combined with home-made monomeric type I rat tail collagen dissolved in 0.02 M acetic acid neutralized at 4°C with 0.1 M NaOH if necessary. Concentrated DMEM was also added to the mixture to yield a final collagen content of 1 mg/ml. Fluorescent carboxylate microspheres (#15700, Polysciences Inc., Warrington, PA) with a 0.21  $\mu\text{m}$  diameter were also added to the cell/collagen suspension at a final concentration of  $3.64 \times 10^6$  particles/ml. Neutralized solutions were composed of collagen (1.0 mg/ml), fluorescent beads, and cells having the density range from  $10^5$  cells/ml (low density, LD) to  $10^6$  cells/ml (high density, HD).

Prior to mixing cells with collagen solution, a membrane dye was applied to approximately 10% to 30% of the cells. Cells were stained for 30 minutes with

CellTracker™ Green CMFDA (5-chloromethylfluorescein diacetate, Invitrogen Corporation, Carlsbad, CA) diluted 200X in HEPES buffered saline. These fluorescent probes for long-term tracking for living cells and fluorescent chloromethyl derivatives that freely diffuse through the membranes of cells. To maintain normal cellular physiology and reduce potential artifacts, the concentration of the dye should be maintained as low as possible. Therefore, several tests on the range of concentrations were performed to identify an optimal staining concentration of the probe.

### 3.2.2 Testing Device

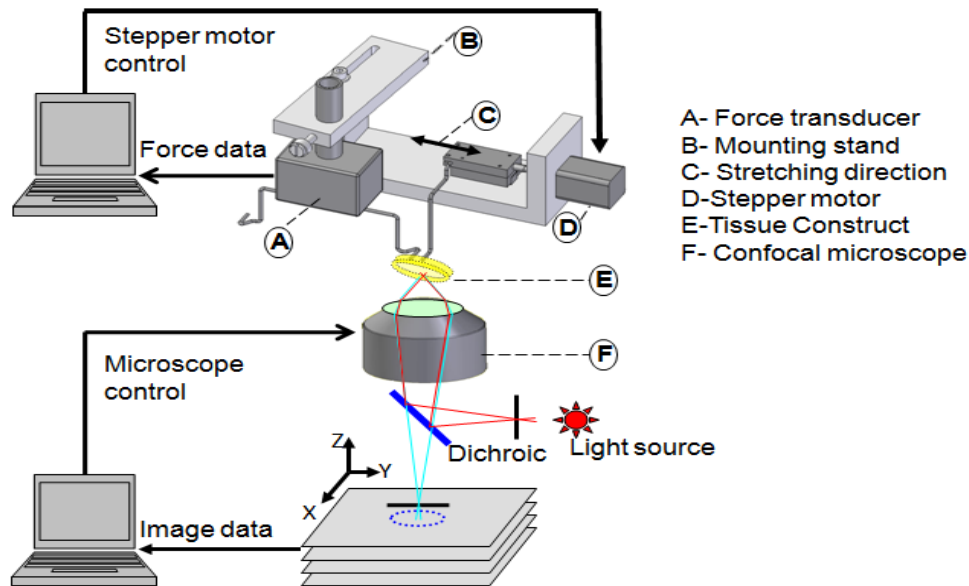


**Figure 3- 1 Testing devices and system diagram**

The responses of contractile fibroblasts to prescribed stretch in 3D culture were probed using confocal fluorescence microscopy and mechanical measurements of active contractile response. The system are composed of two sub-systems. Each sub-system has its own computer to execute specific software. One is used to control the portable

stretcher which has a stepper motor for motion control and a force transducer for force data collection. Another one is the imaging system which is responsible for the position control of confocal microscope and image data collection. The portable stretcher has three major components which are A-force transducer, B-mounting stand and D-stepper motor. The moving direction of stepper motor is labeled as C in the picture. The mounting point of ETC is label as E. Two titanium mounting rods are designed to hold the ETC. One rod is connected to the force transducer. Another one is attached to the stepper motor. After the ETC is mounted to the rod, the imaging system can be refocused to locate the position of stained cells in the 3D space of the ETCs to monitor their dynamic activities when subjected to the external mechanical stimuli from the rod movement.

To simultaneously image living cells inside tissue constructs and measure their stretch-induced mechanical responses, a custom-made tissue stretcher was designed to work over the fluorescence confocal microscope. A computer was used to control the custom-made tissue stretcher which consists of three major subassemblies (Figure 1): (A) an isometric force transducer, (B) a mounting stand, and (D) a linear actuating stepper motor. The isometric force transducer (model 724490, Harvard Apparatus, Holliston, MA) connects to the other end of the tissue through a titanium mounting rod. The linear actuating stepper motor has a resolution of 1.5  $\mu\text{m}$  per step. To make the device capable of stretching the tissue to positions with a tolerance of less than 1.0  $\mu\text{m}$ , an eighth-stepping driver (custom developed by Gavin Perry, Washington University Electronics Shop) was used. Since the stepper motor was unipolar, the card

manipulated the current to each transistor causing the electromagnets to turn the motor only one eighth of a step. We used a computer with custom-made software and Linux-based operation system which sends signals through the digital I/O channels of a PCMCIA card (model DAS16/16-AO, Measurement Computing, Norton, MA) to the stepper motor through the eighth-stepping driver. Software written in the Experix environment (the Experix environment is freeware developed under the GNU license agreement by William B. McConnaughey) simultaneously controlled movement of the stepper motor and acquired force data from the force transducer. Experix programs were written to generate two stretching protocols. One was cyclic stretch which was used in preconditioning of ETCs. Another was a rapid step-stretch, in which ETCs were quickly lengthened and held at that length while the force was monitored for 30 minutes. A second computer was responsible for control of the confocal microscope and acquiring image data.

### **3.2.3 Experimental Protocol**

In each experiment, a ring-shaped ETC was mounted between two titanium mounting rods. The stepper motor (Figure 1C) stretched the ~7mm ETC band (1E) along its circumferential direction. One of the two titanium mounting rods holding the ETC was connected to the force transducer (A), and the other to the stepper motor (B). ETCs were tested on a heating micro-incubator stage to maintain temperature around 37°C; the apparatus was enclosed in a home-built thermal enclosure, and allowed to reach a steady temperature for several hours prior to experimentation. After the ETC

was mounted, the imaging system was refocused to locate the position of stained cells in the 3D space of the ETC to monitor their dynamic activities when subjected to the external mechanical stimuli from the rod movement. The stretching protocol was ten 5% preconditioning stretches applied at 20%/s, followed by a 10% stretch and 30% stretch at 20%/s. 30 was allowed for force relaxation prior to the 10% and 30% stretches. Preconditioning involved application of cyclic mechanical stretch. A long term cyclic mechanical preconditioning might improve the contractility of tissue constructs (Zimmermann, Schneiderbanger et al. 2002; Wille, Elson et al. 2006; Moon du, Christ et al. 2008; Ghazanfari, Tafazzoli-Shadpour et al. 2009), as it improves properties of engineered skeletal muscle tissues *in vivo*. These effects of cyclic stretch are believed to representative of physiological conditions and therefore appropriate precursors to studies involving mechanical stretch of cells. The imaging protocol involved tracking the reconfiguration of cells with a stack of confocal microscopy images taken through their thickness every three minutes.

Temperature control is an important factor when quantifying cellular behavior. Our working temperature could be controlled between 36.5°C and 37.5°C. Associated evaporation of HEPES buffered DMEM, which, if unchecked, occurred at 0.5 ml HEPES solution every 30 minutes could alter the ionic strength of the solution, and the force transducer could be influenced by variable buoyancy. 0.5ml distilled water was added every 30 minutes to maintain the ion strength and keep total volume at 4 ml.



### **3.2.4 Multidimensional imaging of tissue constructs.**

All multidimensional images were taken using the Ziess confocal laser scanning microscope system (Axiovert 200M with LSM 510 ConfoCor 2, Carl Zeiss Inc., Oberkochen, Germany) with argon and helium-neon laser to produce two different channel images. One channel displayed the shape of stained cells as determined by the membrane dye CellTracker Green (excitation wavelength, 488 nm). The other channel imaged the fluorescent beads in experiments for which these were included (excitation wavelength 543nm).

Before taking images, tissue constructs were positioned to center an area of interest within the light path of the objective (e.g. Figure 2). The Z-axis, controlling the focal plane, was perpendicular to the X-Y plane; the position of the focal plane could be manipulated using confocal microscopy. At each focal plane, the confocal microscope scanned to produce a 2D image for each channel. Combinations of 2D images at different equispaced focal planes could be stacked to generate a set of volume data showing cell morphology.

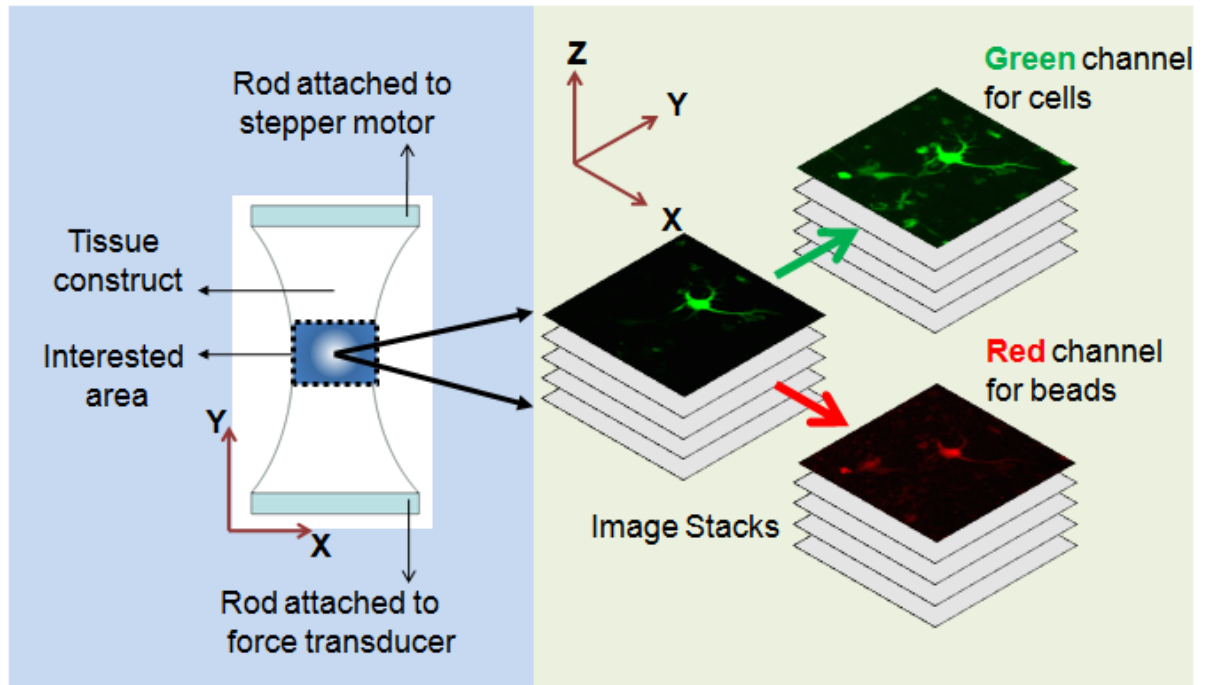


**Figure 3- 2 Illustration of image data processing**

Once ETCs are mounted to the titanium rods of the portable stretcher, at the mounting point, two rods can be moved apart to hold a distance so that the rods only slightly touch the tissue constructs to keep ETCs at the initial length without any stretch. After ETCs have been mounted to the rods; image system can be manipulated to locate the position of stained cell in the interested area. The interested area is shown in the left panel with a rectangle area and surrounded by the dash lines. When taking images of the interested cell, different focused plane produces individual 2D image. Combinations of the 2D images generate 3D image stacks. According to the design requirements on different experiments, the original image stacks may contain more than one channel images. The images from different channels can be separated and recombined as channel based image stacks. For example, green channel is for the cell and the red

channel contains beads information around cells. To reconstruct the shape of cells in the 3D, the green channel of cell channel can be deconvoluted to get rid of blurring effects and get the morphology in the ETCs. The image formation method can be repeated and utilized to monitor cell responses while mechanical stimuli are applied to the ETCs on time varying or specific time frame experiments.

When taking the image stacks in the 3D ETCs, photobleaching was observed, blurring and changing the effective sizes of cells over the time-lapse microscopy. To counteract this in time-lapse monitoring, a calibrated five percent intensity increase was applied in each time frame.

When reconstructing the 3D shape of cell in the ETCs, numerical deconvolution was used to reduce the negative effects on out-of-focus fluorescence. Deconvolution redistributed light to its points of origin in the specimen according to how much the out-of-focus light was expected for the optical system. The characterization of out-of-focus light is based on the 3D image of a point source of light, the so-called point-spread function (PSF). The PSF describes what happens to each point source of light after it passes through the imaging system. Once the PSF has been determined, 3D images of cells inside the ETCs can be deconvoluted to remove systematic errors in data collection. The concept can be illustrated in the Figure 3. In Figure 3A, target object was imaged and convoluted with the PSF image. This produced a blurred image. In Figure 3B, after deconvolution, a sharper image resulted.

Images of beads were analyzed to obtain their locations before and after stretch of the ETC, and standard methods (Legant, Miller et al. 2010) were applied to analyze the average local strain field around cells as a function of the applied strain field.

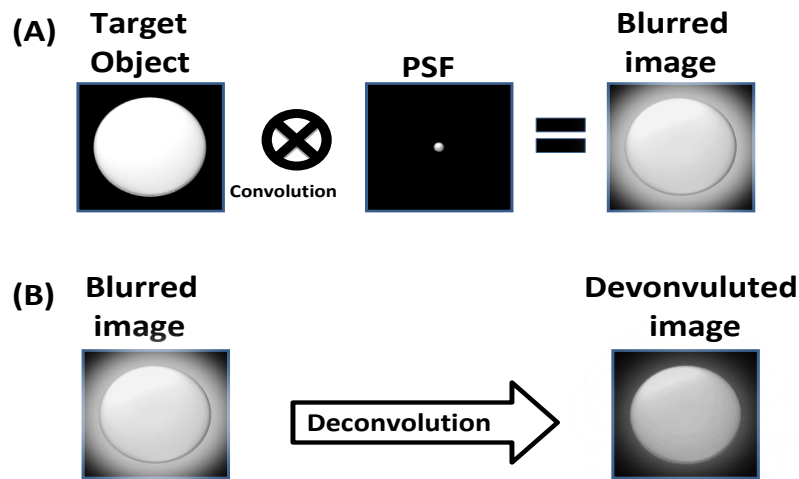


**Figure 3-3 Concept of convolution and deconvolution in the fluorescence image**

This diagram demonstrates the concept of a general deconvolution procedure, where  $\otimes$  represents the convolution operation. The convolution result of object image and the imaging system Point Spread Function (PSF) is commonly influenced by noises and therefore generates the blurred image as shown in the picture A. Blurred images can be processed by deconvolution method to get an improvement on the image quality. Before deconvolution processing, finding PSF is necessary. There are two ways to determine the PSF image of a confocal microscope. One is to calculate and construct theoretical PSF image based on the optical characteristics. Another one is to measure

images from a test body with a known or a regular shape. By using the deconvolution method in reconstruction of 3D spaces, the 3D morphology and dynamic activities of cells in the ETCs can be presented.

## **3.3 Results**

### **3.3.1 Cell Dynamics in the ETCs Can Be Monitored by Membrane Staining**

The membranes of a fraction of cells were stained with CellTracker™ Green to visualize baseline cellular dynamics and cellular responses to mechanical stretch in the ETCs. When cells have been successfully stained with CellTracker™ Green, their dynamics were readily evident within a confocal microscope. In the absence of mechanical stimulus, cells naturally extended and retracted processes reminiscent of filopodia. As in Chapter 2, no lamellipodia-like extensions were evident. The time constant associated with retractions, fitting normalized length of each filopodium to an exponential, was on the order of  $4200 \pm 160$  sec XXX. Cells that were both spindle-like (Figure 3.5; these aligned nominally with the circumferential direction of the molds) and star-like or stellate (Figure 3.4; these showed no preferred orientation) were evident. Retraction rates were independent of cell morphology. Cells cultured at low concentration tended to display a stellate shape. In contrast, cells cultured at high concentration tended to display a spindle-like morphology.

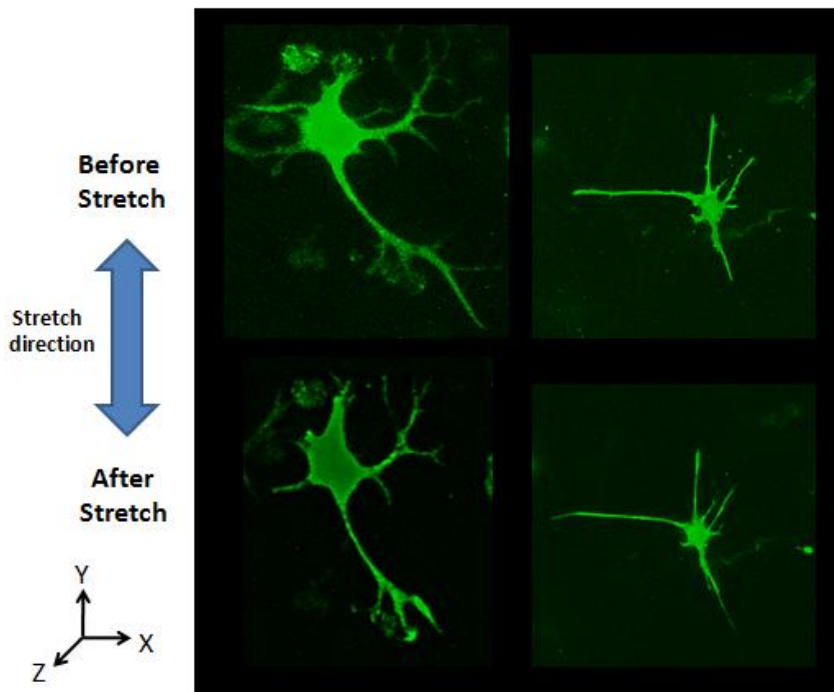
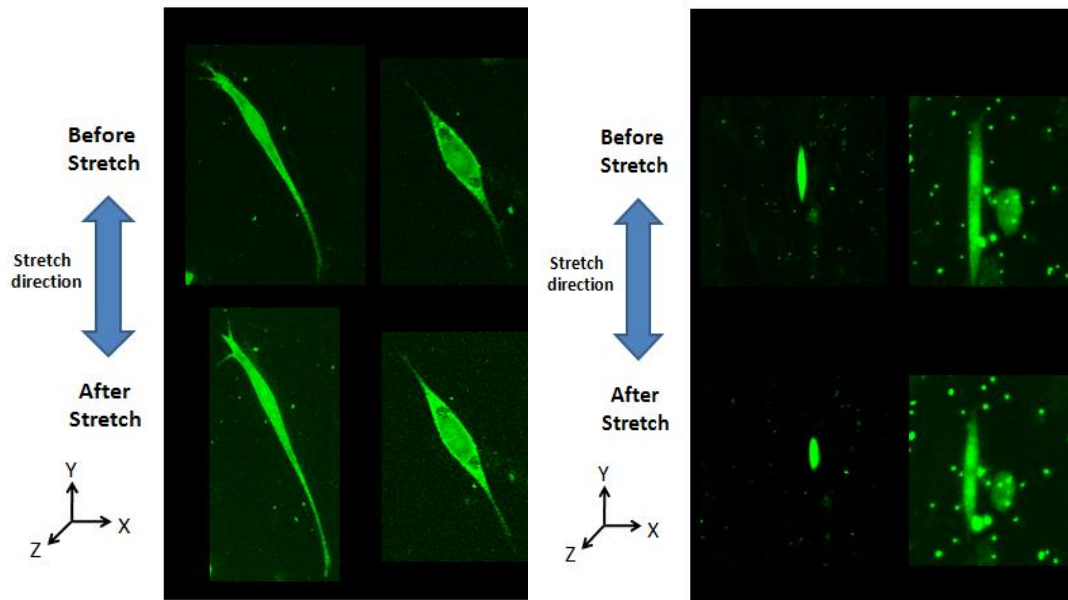


**Figure 3- 4 Star-like(stellate) cell in response to mechanical stretch**

At low cell concentration in the ETC, shapes of cells are more star-like (“stellate”). The images are taken from the ETCs before and after external mechanical stimuli are applied to them. Stretch direction is in the Y axis direction. The images shown here are the projection images of 3D image stacks. There are two different cells are shown to display the morphology change of stellate cells before and after stretch. The top two images show the original morphology before the stretch. The bottom two images show morphology of the same cells after being stretched and held for a certain period of time. The observation shows that stellate cells extend processes in the direction of stretch. However, stellate cells release processes in the directions perpendicular to stretch. This shows cells are sensitive to the direct mechanical stimuli.



A. Cells remain attaching to the ECM    B. Cells detach from ECM

**Figure 3- 5 Spindle-like cell in response to mechanical stretch**

At high cell concentration in the ETC, shapes of cells are more spindle-like. The images are taken from the ETCs before and after external mechanical stimuli are applied to them. Stretch direction is in the Y axis direction. Results show that two obvious but different responses are observed. In picture A, cells remain attaching to the ECM. Therefore, the spindle cells can be elongated with the stretch and hold of the ETCs. In picture B, cells rapidly detach from the ECM. Thus, the spindle cells are retracting after the ETCs are stretched and held for 30 minutes. Spindles typically align in the mold's circumferential direction, which is also the stretch direction in this study.

### **3.3.2 Cells Change Membrane Morphology in Response to Mechanical Stretch**

Following a rapid change in length of the ETC, the isometric force required to maintain the ETC isometrically increased, then decreased viscoelastically and actively, as shown in previous work from our group (Wakatsuki, Kolodney et al. 2000; Zahalak, Wagenseil et al. 2000; Wagenseil, Wakatsuki et al. 2003; Marquez, Genin et al. 2006; Nekouzadeh, Pryse et al. 2007; Nekouzadeh, Pryse et al. 2008; Marquez, Elson et al. 2010). Many cells displayed active responses at the whole-cell level to this stretch.

Both stellate and spindle-like cells displayed elongation along the stretch direction in response to the mechanical stretch. This could in some degree be explained by passive stretch (Figure 3-5A). Analysis of the strain field on analogous ETCs in Chapter 2 showed a nonlinear relationship between ETC strain and local strain around cells in the focal regions, and showed variations in the mechanical environment around individual cells. At 10% ETC stretch, the peak local strain around a cell was, on average, approximately 5%; at 30% ETC stretch, the peak local strain around a cell was, on average, approximately 10%. Observations showed that some cells responded to the mechanical stretch with active retraction involving detachment from the ECM and shortening along an axis nominally parallel to that of the mechanical stretch (Figure 3-5-B). Other cells remained attached and extended processes parallel to the direction of mechanical stretch (Figure 3-4A and Figure 3-5A). Stellate cells with processes perpendicular to the stretch direction retracted processes perpendicular to the stretch direction, and extended into the stretch direction. Some cells extended processes that



were initially perpendicular to the stretch direction by extending the process at approximately 45° to the stretch direction; this processes were typically smaller in diameter and could be best resolved following deconvolution of each individual image in a stack, then reconstruction (Figure 3-6).

## Comparisons of blurred and deconvoluted images after 10% stretched and held

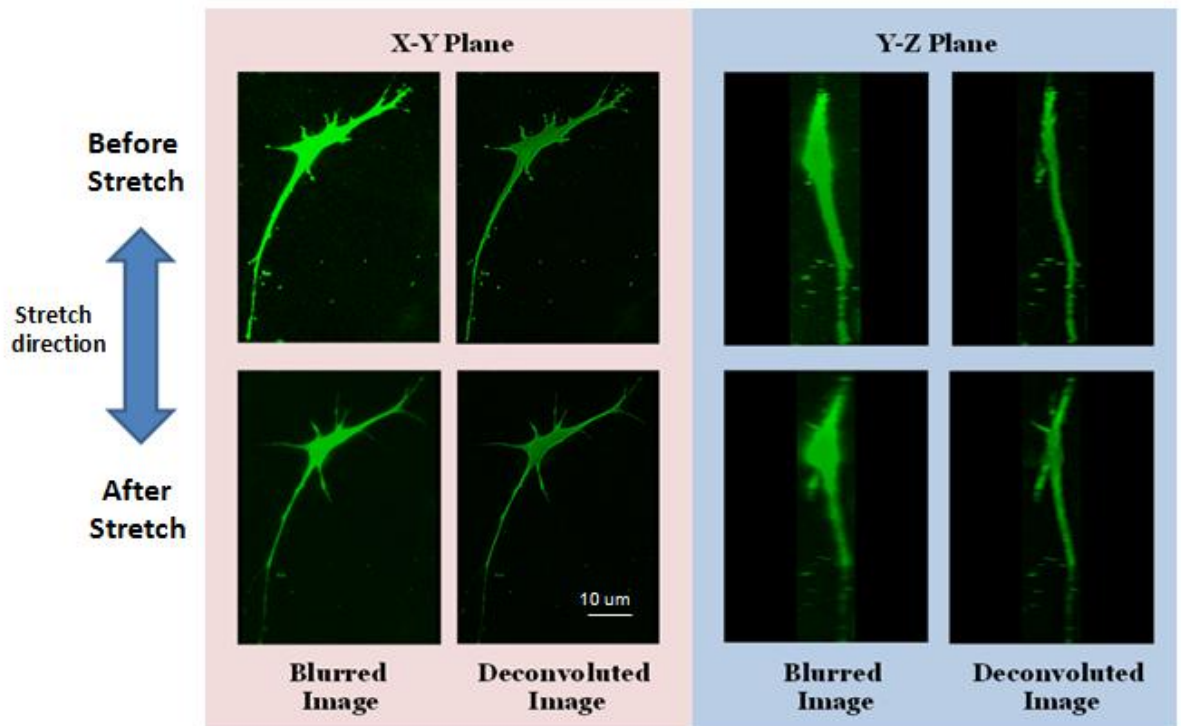


**Figure 3- 6 Morphological reconstruction of cells in response to the mechanical stretch**

Cells morphologies in the ETCs are presented before and after external mechanical stimuli are applied to them. Y axis stands for the stretch direction. To determine 3D

cell morphology, deconvolution method is also used to compare the morphology changes before and after stretch in the X-Y plane and Y-Z plane. 3D cell morphology is reconstructed by either the original or the deconvoluted image stacks. The results are shown in X-Y plane and Y-Z plane separately.

Deconvoluted images showed significantly different in the Y-Z plane instead of X-Y plane. This is because of the blur in Z is much greater than the blur in X and Y. Or the resolution of confocal microscope in the X and Y axis is higher than the resolution in the Z axis.

### **3.3.3 Rates of Stretch-Induced Process Retractions Were Stretch-Independent, and Were Faster Than Process Retractions in the Absence of Stretch**

Image stacks that bounded individual cells were projected into 2D images to simplify quantitative analysis of morphological changes to cellular processes. Using this technique, dynamic alterations of morphology were recorded as time series videos (see Supplemental Movies 1 and 2). In this study, morphological changes in different cells in different ETCs experiencing four different loading conditions were monitored over time. The dynamic variation of the normalized lengths of cell processes following mechanical stretch was then calculated from the videos (Figure 3-7). For cells in the control group in ETCs that received no external stretch (cross symbol, Figure 3-7), retraction and extension of processes occurred with a time constant of  $4100 \pm 100$  s. In cells tested by a preconditioning procedure followed by a 10% rapid ETC stretch and isometric hold of the ETC (diamond symbol, Figure 3-7), the retraction of processes

was more rapid, with a highly variable time constant on the order of 2900 s with a very high standard deviation (Figure 3-8); recall that the nominal peak principal strain around a cell under this ETC loading condition was approximately 5%. For cells tested following this same protocol but without a preconditioning procedure applied to the ETC (square symbols, Figure 3-7), no discernable change in time constant was evident. Some cells tested by preconditioning followed by a 30% rapid ETC stretch and isometric hold of the ETC (recall that this corresponded to a 10% peak principal strain in the vicinity of the cells imaged) displayed a slightly faster retraction rate (triangular symbols, Figure 3-7), with a time constant of 1500 s, but this difference was not significant statistically. Time constants in cells in stretched tissue constructs were significantly different from those in the control group, especially at the 10% cellular stretch level. The time constants were not significantly different from time constants measured for cytoskeletal rearrangements in Chapter 2.

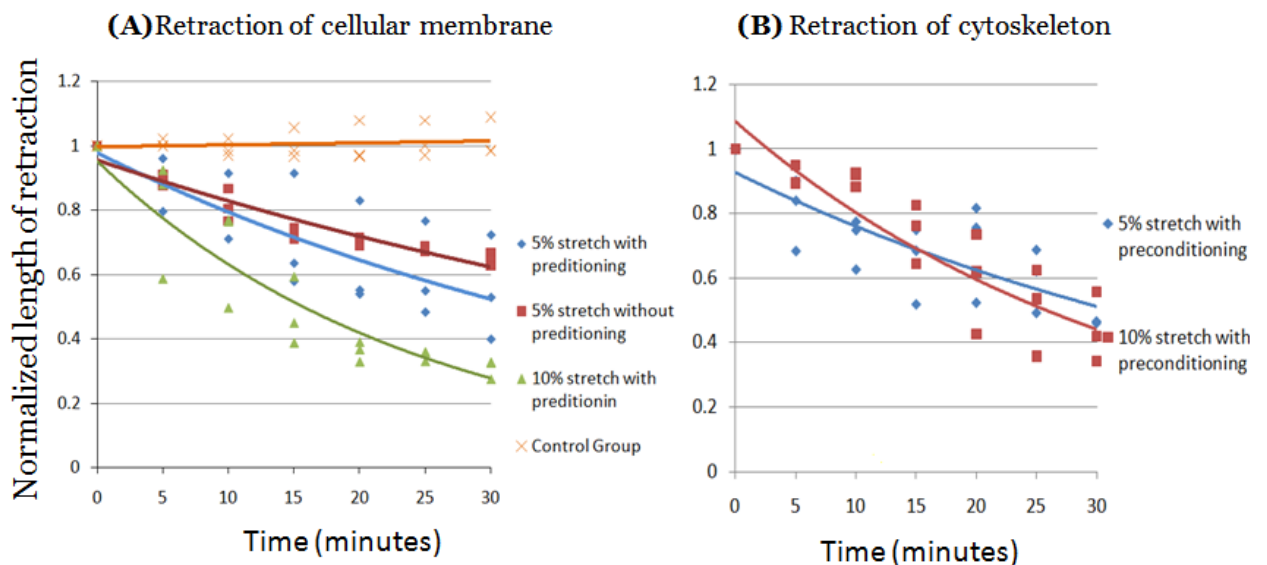


**Figure 3- 7 Retraction of plasma membrane and cytoskeleton in response to the mechanical stretch**

Cell membrane retraction shows that cells are sensitive to external mechanical stimuli

(A) The cross mark is the control group without any preconditioning and stretch. The diamond mark is the group with preconditioning before the 5% stretch. The square mark is the group without preconditioning before the 5% stretch. The triangle mark stands for the group with preconditioning before 10% stretch. 10% stretch produced the maximum retraction with time. (B) Measurements of retraction from the cytoskeleton alterations displayed a similar pattern as shown in the (A) from the plasma membrane. The number in each case on retracting response of time series is  $n=3$ .

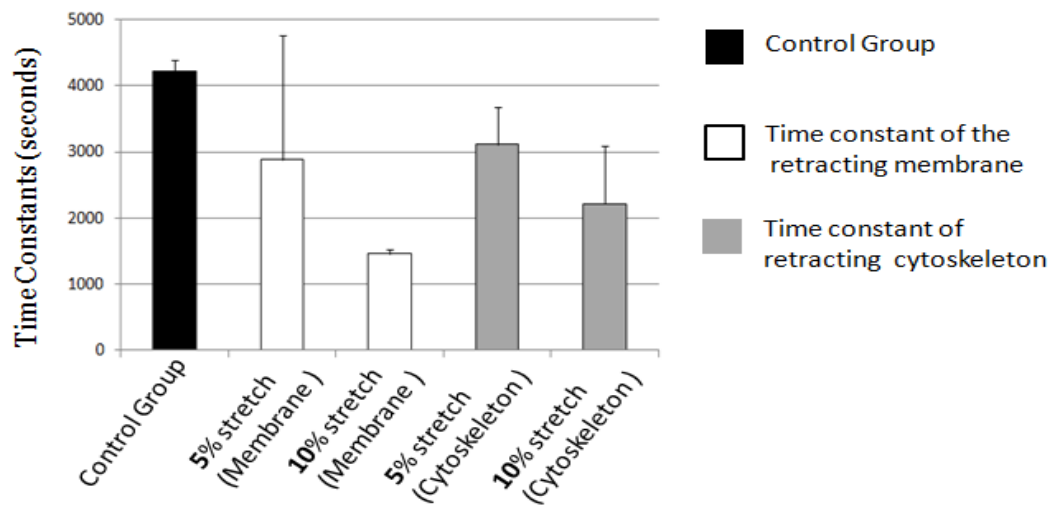


**Figure 3- 8 Time constants of cellular dynamics in response to mechanical stretch.**

Control group (black, mean  $\pm$  standard deviation :  $4200 \pm 160$  sec) represented no preconditioning stretch before the 5% stretch. Preconditioning was performed in both membrane- (white) and cytoskeleton-stained (gray) groups. Two stretch levels (5% and

10%) were examined in both membrane and cytoskeleton groups. This graph showed two trends. First, preconditioning decreased the time constant associated with retraction of cytoskeletal processes in response to mechanical stretch. Second, although increasing the magnitude of stretch (10% vs. 5%) decreased the time constants, these changes were not significant statistically. The time constants of membrane process retraction were  $2900 \pm 1900$  sec for 5% stretch and  $1500 \pm 70$  sec for 10% stretch. The time constants of cytoskeletal rearrangements were  $3100 \pm 560$  sec for 5% stretch and  $2200 \pm 870$  sec for 10% stretch.

## **3.4 Discussion**

### **3.4.1 Cells Respond Actively to Mechanical Perturbation of Their Environment**

The cells observed in this study actively remodeled their extracellular environment, and responded to changes in it. Cell morphology was a function of culture conditions, with cells cultured in a lower cell density tending towards a stellate shape, and those cultured in a higher cellular density tending towards an aligned, spindle-like shape. Filopodia-like processes were evident, but lamellipodia-like processes were not. In response to mechanical stretch, cells tended to retract processes perpendicular to the direction of stretch and extend processes in the direction of stretch. Cells with processes perpendicular to the direction of mechanical stretch sometimes extended these processes or branched these processes in a direction between the direction of the process and the direction of loading.

Retraction of cellular processes following mechanical stretch occurred more rapidly than did retraction or extension of cellular processes in the absence of mechanical stretch. Time constants associated with retraction were many orders of magnitude slower than those associated with tether retraction in a leukocyte and were not statistically different from those associated with cytoskeletal remodeling, suggesting either that cytoskeletal remodeling was a rate-limiting factor in membrane retraction, or that membrane retraction occurred in concert with cytoskeletal rearrangement. Note that 10% cellular stretches were applied only after 5% cellular stretches in all experiments. Therefore, the statistically insignificant differences in mean time constants observed as a function of stretch in this study should not be over-interpreted, and the data support the idea that retraction of processes occurs at a rate that is independent of strain.

### **3.4.2 A Coupled Imaging and Mechanical Measurement System Can Be Applied to Quantify Cellular Responses to Mechanical Stretch**

To monitor cell dynamics in response to mechanical stretch, several technical challenges, including system synchronization and synthesis of ETCs, were addressed, evaluated, and controlled.

#### **3.4.2.A System Synchronization**

When collecting data, two different computers were used to acquire image and force data. This produced a synchronization problem because of delays from data communications and manual operations. The delay came from manually tracking the same cell before and after stretch of an ETC. Also, following rapid stretch of an ETC, target cells moved slightly out of the focal plane because of ETC deformation. Therefore, time was required to track the cell of interest. To improve synchronization, a controlled time delay of between one and two minutes was applied uniformly.

#### **3.4.2.B Synthesis of Homogeneous ETCs**

When preparing ETCs, air bubbles and differential remodeling could lead to non-homogeneous properties and local mechanical environments of ETCs. The latter is an unavoidable feature of implanting living cells at random in an environment that they can manipulate. The advantage of this environment is that cells can manipulate it in a natural way; the disadvantage compared to synthetic extracellular matrix materials (Legant, Miller et al. 2010) is that the resulting local strain fields can be highly non-uniform. This might underlie the diversity of cellular responses observed in this study.

The issue of entrained and random air bubbles was addressed using three different approaches. The first was a vacuum method: decreasing the air pressure in a tube containing the cell solution reduced the concentration of air. However, care had to be taken to prevent over-vacuuming, in which reduction of the concentration of carbon

dioxide is harmful to cells in the culture environment. The second was centrifuging the cell solution before collagen polymerization, which reduced residual air inside the cell solution. However, some cells did not survive the spinning down process. The third approach, and that found most feasible, was to simply allow the cell solution to sit at room temperature for 10 to 15 minutes extra before pouring the cell solution into the molds, allowing residual air to float up to the surface of the cell solution, and subsequently drawing cell solution from the bottom of the container.

### **3.4.2.C Initial Length of the ETCs**

Relating nominal strain of an ETC to local strain around individual cells is a challenge because of randomness within ETCs, and because of structural challenges in the testing of a soft ETC ring. In the latter problem, determining the initial length of gel is difficult because of the compliant and viscous nature of the gels (Pryse, Nekouzadeh et al. 2003). Here we defined un-stretched length of an ETC as half of its circumference. Ideally, ETCs incubated with same method and environment should present identical geometry. However, cells inside the ETCs may behave differently, and initial un-stretched lengths of ETCs may vary; however, initial un-stretched lengths were similar for ETCs made simultaneously. Even in this case, ensuring a slight contact with both titanium bars of the loading apparatus was challenging. We achieved this by monitoring the force transducer, which was feasible because we tested only one ETC at a time: a force increase indicated mechanical contact between bars and ETC, and the



bars would be reset to begin the test at a prescribed stretch rate. Application of this method relies upon having a sufficiently sensitive force transducer.

#### **3.4.2.D Cellular Staining**

Effective staining of cell membranes for cells in ETCs involved deviations from standard procedures for CellTracker™ Green. Three factors were optimized. First, the concentration of dye was tested over a wide range of concentrations to identify conditions that maintained normal cellular physiology. A high concentration of dye led to cell death, sometimes after several days of ETC incubation. Second was the cell type. The CEFs used could retain the dye for a week, but other cell types could actively efflux the dye in minutes. The last was the gel solution environment. DMEM without phenol red, the PH indicator, was used because phenol red may quench the fluorescence of the dye. Although residual FBS and trypsin present may also have similar negative effects, eliminating phenol red eliminated this problem.

#### **3.4.2.E Image Deconvolution**

Deconvolution of the PSF was required to sharpen images. There are two ways to determine the PSF of a confocal microscope. One is to perform a theoretical calculation of the optical characteristics, such as lenses, wavelength, etc. Another is measuring the PSF from an image from a test body. Two major reasons not to use a theoretical PSF (McNally, Karpova et al. 1999; Wallace, Schaefer et al. 2001; Tan, Sendemir-Urkmez et al. 2004; Sarder and Nehorai 2006; Tan, Vinegoni et al. 2007) are

that they are not perfect models, and that theoretical PSF packages may misfit the distribution of blur in the raw image because of idealizations of both axial and rotational symmetry; an empirical PSF contains much more information than in the theoretical models. However, in our studies, the experimentally measured PSF had resolution too coarse to be optimal for cell images of the poor resolution in the Z axis. Only one slice of the experimental PSF image could be utilized to for deconvolution. Therefore, the theoretical PSF was utilized in deconvolution.

### **3.5 Conclusions**

Living cells in an ETC exhibit dynamic responses to changes in their mechanical environment. Stellate cells, evident in ETCs with lower cell density, and spindle-like cells, evident in ETCs with higher cell density, extended and retracted filopodia-like but not lamellipodia-like processes. Following mechanical stretch of an ETC, cells tended to retract processes perpendicular to the direction of stretch and extend processes in the direction of stretch. The diversity of cellular responses might be attributed to randomness associated with remodeling of ETCs. Retraction of cellular processes occurred more rapidly following mechanical stretch, but was independent of the stretch magnitude over the range studied. Results suggest that the cytoskeleton and membrane retract at the same rate during cellular remodeling, and comparison to measurements of membrane retraction in leukocyte tethers suggests that the membrane is resisted heavily during this process.

### 3.7 References

- Chen, Y., G. Girdhar, et al. (2007). "Single membrane tether extraction from adult and neonatal dermal microvascular endothelial cells." Am J Physiol Cell Physiol 292(4): C1272-1279.
- Chen, Y., D. K. Yao, et al. (2010). "The constitutive equation for membrane tether extraction." Ann Biomed Eng 38(12): 3756-3765.
- Ghazanfari, S., M. Tafazzoli-Shadpour, et al. (2009). "Effects of cyclic stretch on proliferation of mesenchymal stem cells and their differentiation to smooth muscle cells." Biochem Biophys Res Commun 388(3): 601-605.
- Girdhar, G. and J. Y. Shao (2004). "Membrane tether extraction from human umbilical vein endothelial cells and its implication in leukocyte rolling." Biophys J 87(5): 3561-3568.
- Girdhar, G. and J. Y. Shao (2007). "Simultaneous tether extraction from endothelial cells and leukocytes: observation, mechanics, and significance." Biophys J 93(11): 4041-4052.
- Kalluri, R. and M. Zeisberg (2006). "Fibroblasts in cancer." Nat Rev Cancer 6(5): 392-401.
- Legant, W. R., J. S. Miller, et al. (2010). "Measurement of mechanical tractions exerted by cells in three-dimensional matrices." Nat Methods 7(12): 969-971.
- Liu, B., C. J. Goergen, et al. (2007). "Effect of temperature on tether extraction, surface protrusion, and cortical tension of human neutrophils." Biophys J 93(8): 2923-2933.
- Marquez, J. P., E. L. Elson, et al. (2010). "Whole cell mechanics of contractile fibroblasts: relations between effective cellular and extracellular matrix moduli." Philos Transact A Math Phys Eng Sci 368(1912): 635-654.
- Marquez, J. P., G. M. Genin, et al. (2006). "Cellular and matrix contributions to tissue construct stiffness increase with cellular concentration." Ann Biomed Eng 34(9): 1475-1482.
- McNally, J. G., T. Karpova, et al. (1999). "Three-dimensional imaging by deconvolution microscopy." Methods-a Companion to Methods in Enzymology 19(3): 373-385.
- Moon du, G., G. Christ, et al. (2008). "Cyclic mechanical preconditioning improves engineered muscle contraction." Tissue Eng Part A 14(4): 473-482.
- Nekouzadeh, A., K. M. Pryse, et al. (2007). "A simplified approach to quasi-linear viscoelastic modeling." J Biomech 40(14): 3070-3078.
- Nekouzadeh, A., K. M. Pryse, et al. (2008). "Stretch-activated force shedding, force recovery, and cytoskeletal remodeling in contractile fibroblasts." J Biomech 41(14): 2964-2971.
- Pryse, K. M., A. Nekouzadeh, et al. (2003). "Incremental mechanics of collagen gels: new experiments and a new viscoelastic model." Ann Biomed Eng 31(10): 1287-1296.
- Sarder, P. and A. Nehorai (2006). "Deconvolution methods for 3-D fluorescence microscopy images." Ieee Signal Processing Magazine 23(3): 32-45.

- Tan, W., A. Sendemir-Urkmez, et al. (2004). "Structural and functional optical imaging of three-dimensional engineered tissue development." Tissue Engineering 10(11-12): 1747-1756.
- Tan, W., C. Vinegoni, et al. (2007). "Imaging cellular responses to mechanical stimuli within three-dimensional tissue constructs." Microscopy Research and Technique 70(4): 361-371.
- Wagenseil, J. E., T. Wakatsuki, et al. (2003). "One-dimensional viscoelastic behavior of fibroblast populated collagen matrices." J Biomech Eng 125(5): 719-725.
- Wakatsuki, T., M. S. Kolodney, et al. (2000). "Cell mechanics studied by a reconstituted model tissue." Biophys J 79(5): 2353-2368.
- Wallace, W., L. H. Schaefer, et al. (2001). "A workingperson's guide to deconvolution in light microscopy." Biotechniques 31(5): 1076-+.
- Wille, J. J., E. L. Elson, et al. (2006). "Cellular and matrix mechanics of bioartificial tissues during continuous cyclic stretch." Ann Biomed Eng 34(11): 1678-1690.
- Yu, Y. and J. Y. Shao (2007). "Simultaneous tether extraction contributes to neutrophil rolling stabilization: a model study." Biophys J 92(2): 418-429.
- Zahalak, G. I., J. E. Wagenseil, et al. (2000). "A cell-based constitutive relation for bio-artificial tissues." Biophys J 79(5): 2369-2381.
- Zimmermann, W. H., K. Schneiderbanger, et al. (2002). "Tissue engineering of a differentiated cardiac muscle construct." Circ Res 90(2): 223-230.

# Chapter 4 : Focal Adhesions in Three Dimensional Tissue Constructs

## 4.1 Introduction

Focal Adhesions (FAs) appear in many adherent cell types and are specialized multi-molecular complexes of the plasma membrane that facilitate cellular attachment to the extra cellular matrix (ECM). At FAs, actin filaments are bound to transmembrane receptors of the integrin family (Hynes 1987), through a complex of structural 'plaque' proteins including vinculin (Geiger 1979) and talin (Burrige and Connell 1983), and involving  $\alpha$ -actinin (Lazarides and Burrige 1975; Kanchanawong, Shtengel et al. 2010).

FA assembly involves both cell signaling (e.g. activation of RhoA or the unfolding of talin to reveal cryptic binding sides for vinculin (del Rio, Perez-Jimenez et al. 2009)) and the stimulation of contractility (force transmission). FAs are dynamic (Wolfenson, Lubelski et al. 2009), and their assembly, disassembly and dispersion may oppose or mitigate pathways associated with tissue remodeling, wound repair, and cell physiology, including cell migration, growth, survival and differentiation (Geiger and Bershadsky 2002; Wolfenson, Henis et al. 2009).

Mechanical loading of cells has been shown to affect cell proliferation, and ECM gene and protein expression, depending on cell types and loading conditions (Wang and Thampatty 2006). Recent studies of cellular responses to mechanical stimuli show force to be a factor that increases integrin expression, activity, and actin polymerization at FAs (Paszek, Zahir et al. 2005; Sawada, Tamada et al. 2006; Hirata,

Tatsumi et al. 2008). One study suggests that cyclic mechanical stretch promoted the formation of FAs, and that these are randomly distributed (Shikata, Rios et al. 2005). A study of cells embedded in collagen showed FA proteins to be related to the regulation of cell speed and persistence in cellular protrusion and matrix remodeling (Fraleley, Feng et al. 2010). Finally, collagen crosslinking and ECM stiffening promote FAs and the invasion of tumor cells (Levental, Yu et al. 2009). These studies indicate that FAs are related to the mechanical properties of the cellular environment, and provide a foundation for understanding how both physiologic and pathologic cellular functions are regulated by FAs and mechanical stimuli.

However, compared to cells cultured in a conventional 2D environment, cells embedded in a 3D matrix show a diffuse distribution of FA proteins, and smaller accumulations of these. The dynamic (turnover) processes of FAs in are now understood in a 2D environment, but FA dynamics in a 3D environment are unknown (Wolfenson, Lubelski et al. 2009). Even their existence has been a subject of debate: one recent study showed rare or no aggregations of FA proteins in a 3D matrix (Fraleley, Feng et al. 2010), while another (Kubow and Horwitz 2011) indicated that these were small but ubiquitous when background fluorescence was adjusted properly. Our results show that relatively large FAs exist in 3D constructs as well. These are evident only in the early in remodeling of a tissue construct. To better understand the dynamic interactions of cells in a force-stimulated 3D environment, we modified the experimental environment of the previous chapters, redesigned testing protocols and utilized our well-established platform of engineered tissue constructs to focus on FAs in a 3D culture environment. We hypothesized that large FAs are associated with

remodeling of compliant tissue regions, especially during the early stages of remodeling. This chapter presents the methods developed to test this hypothesis and a suite of preliminary results.

## 4.2 Materials and Methods

### 4.2.1 Preparation of Engineered 3D Tissue Constructs

Chicken embryo fibroblast (CEF)-populated collagen matrices were made to closely mimic a physiological 3D environment. CEFs isolated from 10-day chicken embryos (Fertile White Leghorn Chicken Eggs, Sunrise Farms, Catskill, NY) were maintained in Dulbecco's modified Eagle's medium (DMEM) with 10% fetal calf serum (FCS), penicillin and streptomycin at 50 units/ml and 50  $\mu\text{g}/\text{ml}$  respectively. Approximately 3% to 5% of the cells were transfected with vinculin GFP. The CEFs in 10% FCS DMEM were then combined with home-made monomeric type I rat tail collagen dissolved in 0.02 M acetic acid neutralized at 4°C with 5-10  $\mu\text{l}$  1N NaOH. Concentrated DMEM was also added to the mixture to yield a final collagen content of 1 mg/ml. Neutralized solutions were composed of collagen (1.0 mg/ml) and cells having the density range from  $10^5$  cells/ml (low density, LD) to  $10^6$  cells/ml (high density, HD). The mixtures of cell seeded collagen gel were then poured in the mold to form ETCs or dropped on the culture dishes to generate the button gels.

Finally, ring-shaped tissue constructs were synthesized using techniques described in the previous chapters, but with a small fraction of cells transfected with GFP-

vinculin. These were subjected to cyclic loading on the stretching device described at a frequency of  $< 1$  Hz and a magnitude of 10% elongation.

### **4.2.2 Transfection of GFP-Vinculin**

Cells were grown in Petri dishes until they reached 60–80% confluence. The cells were detached with trypsin/EDTA and, in suspension, transiently transfected with a GFP-vinculin construct (kindly provided by John Cooper, Department of Molecular Biology, Washington University School of Medicine, USA) using the Cell Line Nucleofector Kit (LONZA Cologne AG). The transfection procedure was followed according to the manufacture's protocol. To identify the vinculin peptide without affecting cellular physiology dynamics, transfected cells were seeded on Petri dishes and cultured for 48h at 37°C and 5% CO<sub>2</sub>.

### **4.2.3 Microscopic Measurement of GFP-Vinculin**

To microscopically analyze GFP-vinculin transfected cells, the fibroblast populated collagen matrices were transferred to a Lab-Tek 8-well chambered cover glass (Nalge Nunc International, Naperville, IL, USA) with complete medium to observe the cells in an LSM 510 LSM510 confocal laser scanning microscope (Carl Zeiss Jena). Each live cell was scanned in one optical plane in the collagen surrounded environment and images were taken in intervals of 10 min for 1 h. A temperature of 37°C was maintained with a heating thermal stage (TRZ 3700, Carl Zeiss, Jena, Germany) during the



observation time. We used a 20X objective and an excitation wavelength of 488 nm with long-pass 515 nm filter.

#### 4.2.4 Fluorescence Photobleaching Recovery (FPR)

Fluorescence photobleaching recovery (FPR) studies were conducted on live fibroblasts expressing GFP-tagged vinculin. A LSM510 confocal laser scanning microscope (Carl Zeiss Jena) with a 20X objective was used with an argon laser ( $\lambda=488$  nm) as excitation source. Regions of interest (ROIs) containing one or several focal adhesions were bleached for 1-5 sec by high-intensity laser application. The time course of the fluorescence recovery of GFP-vinculin was tracked by an attenuated monitoring beam for 130 sec. Fluorescence intensity differences between unbleached ROI and adjoining bleached ROI were calculated and used for an exponential curve fitting to estimate recovery times of GFP-tagged vinculin.

For determination of the recovery half-life, a normalized recovery curve  $f(t)$  is often fitted to a single exponential recovery model using the equation:  $f(t) = A(1 - e^{-t/\tau})$ , where  $A$  is the final value of recovery intensity of fluorescence,  $\tau$  is the fitted time constant and  $t$  is the time after the bleaching pulse. However, fitting of the experimental data obtained required that this fitting function be adjusted to include three time constant components:

$$f(t) = A(1 - Be^{-t/\tau_1})(1 - Ce^{-t/\tau_2})e^{-t/\tau_3}$$

(1)

Here,  $\tau_1$  and  $\tau_2$  are time constants associated with the two recovery timescales;  $A$ ,  $B$ , and  $C$  represent total recovery following the initial photobleaching pulse, and  $\tau_3$  represents the timescale for photobleaching or another factor that leads to reduction in signal intensity over scanning of the region of interest during the course of the experiment.

All data were corrected for photobleaching prior to curve-fitting in the following way (Figure 4-1). In each image, the fluorescence intensity of a FA in the same cell but that was not photobleached was also measured to identify the rate of fluorescence decay associated with fluorescence photobleaching associated with scanning. Then data from within the ROI were normalized by these data from the second FA. Although this might not capture effects of photobleaching with perfect accuracy, the fitting function in Equation (1) contains sufficient flexibility to account for any error.

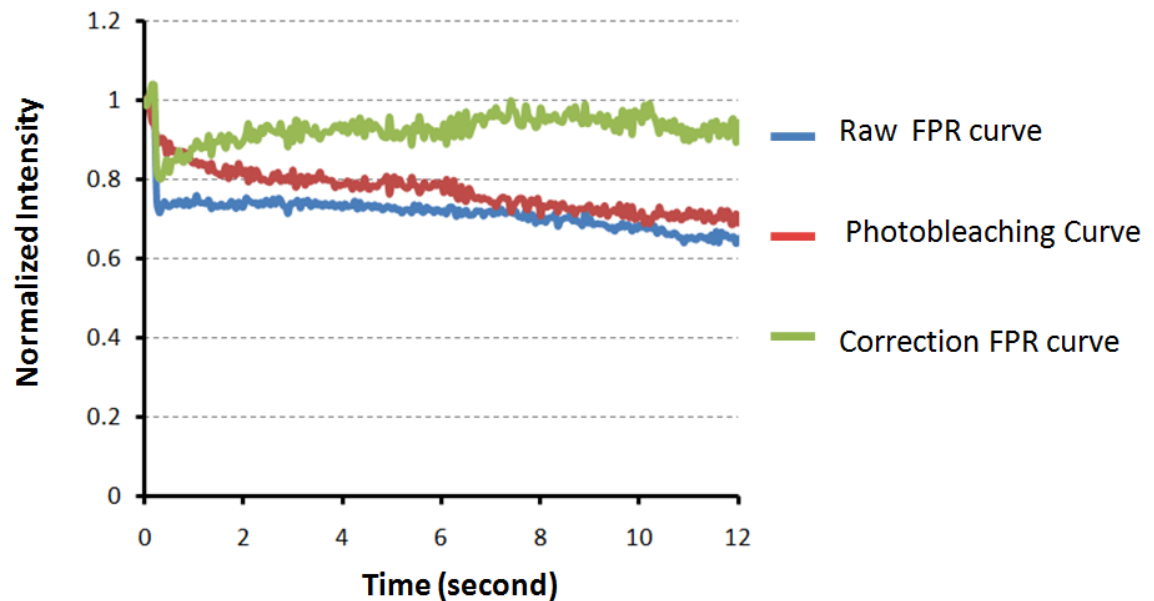


Figure 4- 1 Original and corrected FPR curve

Realistic FPR curve (green), raw FPR curve (blue) was corrected by the photobleaching curve (red). The temporal resolution is 50ms.

## 4.3 Results

### 4.3.1 Larger Focal Adhesions Exist in Tissue Constructs Early in Remodeling

Cells transfected with vinculin–GFP and cultured in our 3D tissue culture environment generated FA patterns similar to those seen in 2D culture. For example, in the field of cells shown (Figure 4-2A, in which the green-transfected vinculin GFP is superimposed upon brightfield imaging of cells in grey), FA patches are evident in a great many cells. A few cells appearing as large green patches were dead. Even the two cells in the center that appear to present only diffuse vinculin-GFP at low magnification show more FAs representative of those seen in 2D culture when magnified, with elongated patches evident (Figure 4-2B).

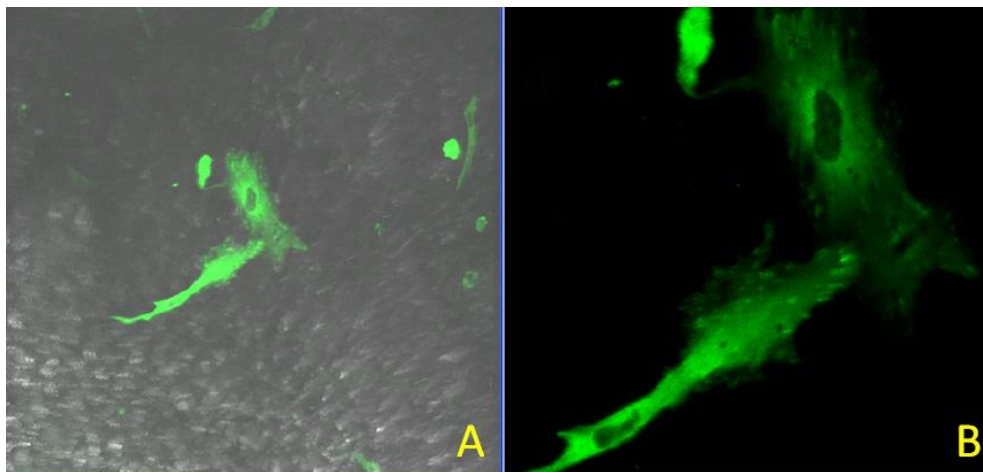
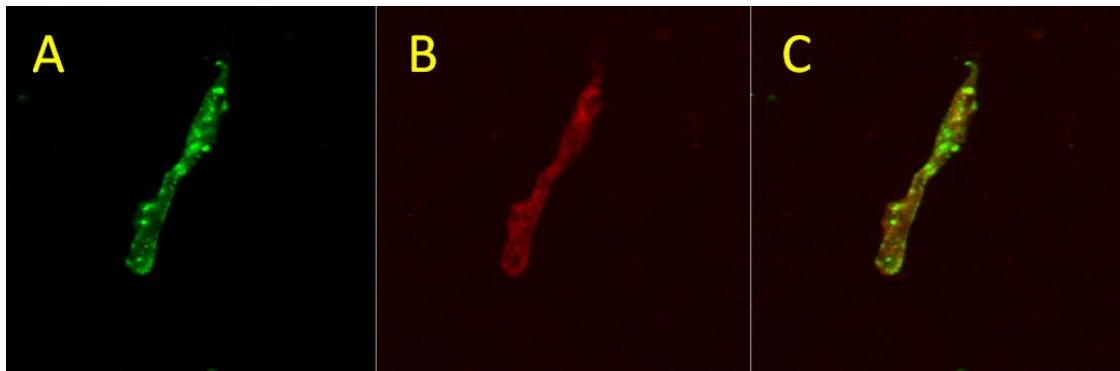


Figure 4- 2 Focal adhesions in button gels

Vinculin-transfected cells (green) were cultured in tissue-construct-like button gels. The transfected cells are embedded in the collagen matrices as shown (A). When zooming in, the transfected cells displayed focal adhesion patterns analogous to those seen in 2D culture.

In general, FAs within cells were less oblong than the FA patches seen typically in 2D culture (e.g. Figure 4-3). To confirm that these patches were indeed FAs, cells transfected with vinculin were further immunolabeled by paxillin. The patterns matched well, although the patches corresponding to vinculin were smaller in size than those corresponding to paxillin (Figure 4-3B&C).



**Figure 4- 3 immunolabeling of focal adhesions in ETCs.**

Vinculin-transfected cells (green) were immunolabelled by paxillin (Red). The transfected cell was cultured in the ETC, a realistic 3D environment.

While FA-like accumulations of vinculin were clearly evident in the early stages of ETC remodeling, as shown in the images of Figure 4-4, they were rare or absent in more heavily remodeled tissues. Cells cultured in the 3D collagen matrices for three

days showed no evidence of large FAs regardless of whether they were stellate (Figure 4-4D) or spindle-shaped (Figure 4-4C). Cells in tissue constructs that were subjected to a broad range of mechanical loading regimes using the techniques of the previous chapters, including loading regimes associated with formation of actin stress fibers, also failed to display focal adhesions.

As a control to ensure that the 3D mechanical environment and not the cells were the cause of the absence of FAs, cells that migrated out of the tissue constructs and onto the glass slide were studied. The position of a vinculin-transfected cell which spread and crawled onto the 2D substrate is shown in the Figure 4-4A. In Figure 4-4B, the same cell, pictured away from the tissue-like collagen constructs, displayed a dot-like pattern indicative of mature FAs. This indicated that these cells, in a 2D culture, can spread and attach to hard surfaces and therefore generated large and strong focal adhesions. If FAs existed in the cells when cultured in 3D, they were small in comparison to those generated in the 2D cases.

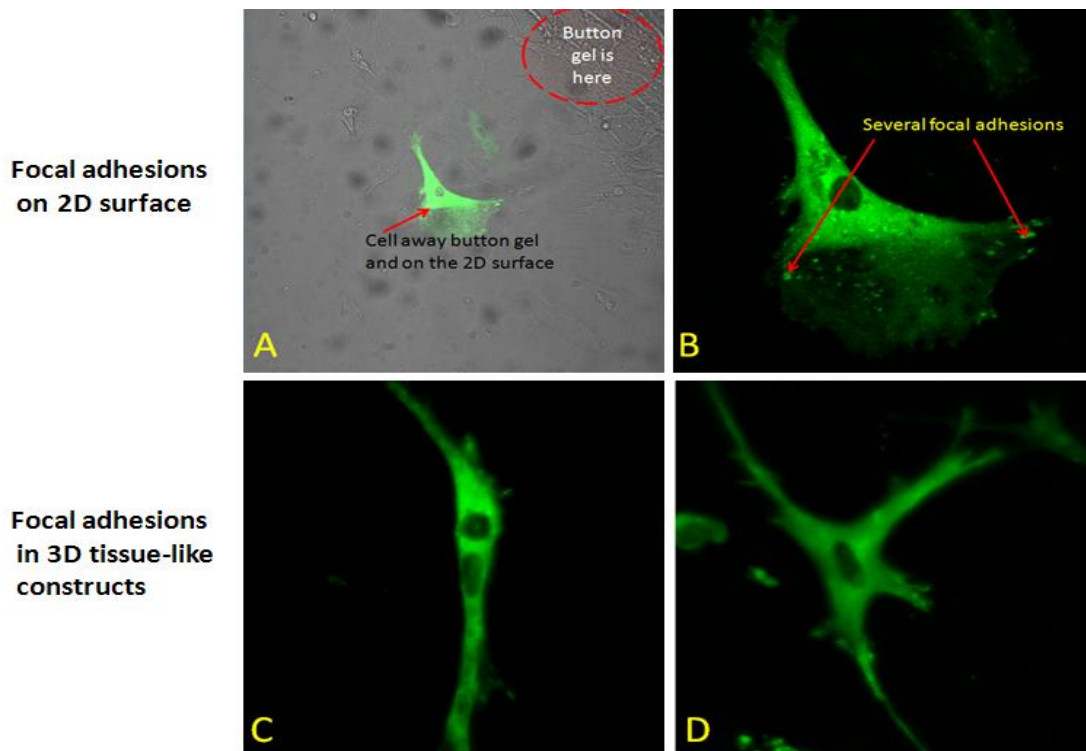


**Figure 4- 4 Comparisons of Focal adhesions between 2D and 3D environment.**

Vinculin-transfected cells (green ) cultured on the 2D substrate showed typical pattern of focal adhesions(A: relative position of cell to the button gel; B: patterns of focal adhesion ). In the tissue-constructs-like environment, vinculin-transfected cells in the shape of spindle-like (C) or star-like(D) displayed small or not noticeable focal adhesions.

Additionally, we have found that large FAs exist in ring-shaped ETCs early in remodeling. These disappear following 30 minutes of cyclic stretch at 10% strain. We therefore hypothesize that remodeling associated with stretch leads to break-up of large focal adhesions.

### 4.3.2 The Remodeling of Collagen and Cells in ETCs

The timing of FA development is variable throughout a tissue construct, although a trend of decreasing FA size over time was observed. We asked whether this might be related to internal structures within the ECM, recognizing that 3D ECMs affect the structural, mechanical and biochemical components of the cellular microenvironment pivotal to cell and tissue development. Although data are not yet conclusive, we developed a system whereby we could test the hypothesis that large FAs correspond to lower or intermediate degrees of collagen remodeling.

In reflectance mode confocal microscopy, collagen fibers of ETCs can be observed directly without staining and provide good axial and lateral resolution. Results show collagen fibers remodeled from a random distribution to an organized structural network that typically aligned with the direction of constraint when present in a ring-shaped ETC, and also connected cells or groups of cells. ETCs after one day of culture were imaged, showing a random distribution of collagen (Figure 4-5A). In a nominally identical tissue construct, a transitional state could be observed (Figure 4-5B). In this picture, the collagen fibers were more organized and began to exhibit a preferred orientation. Finally, a very compact pattern of collagen fibers was demonstrated in Figure 4-5C, taken in the same tissue construct as Figure 4-4B. The compact pattern could be found at a multitude of locations throughout the ETC, not necessarily close to the edge of the ring shaped ETC.

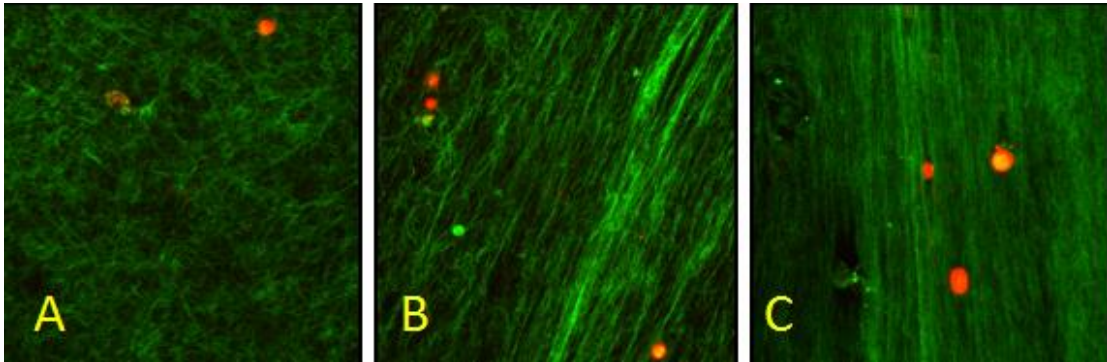


**Figure 4- 5 Remodeling of collagen fibers in ETCs**

Pictures on alignment of collagen matrix were taken in the ETC after one day culture with vinculin-transfected cell (red). The remodeling process of collagen fibers showed randomly distributed fibers become organized and aligned in the circumferential direction preferred by cells.

The process of collagen remodeling seems to be dominated by fibroblasts because they use the ECM to direct and maintain their self renewal and differentiation potential in tissues. During the process, we found that cells establish a network (e.g. Figure 4-6A) that appears to link and organize individual cells in the ECM. We also found several clusters of adjacent cells forming ring-like structures (Figure 4-6B). These were distributed in the ETCs and connected to each other through aligned collagen fibers networks and aligned cells.



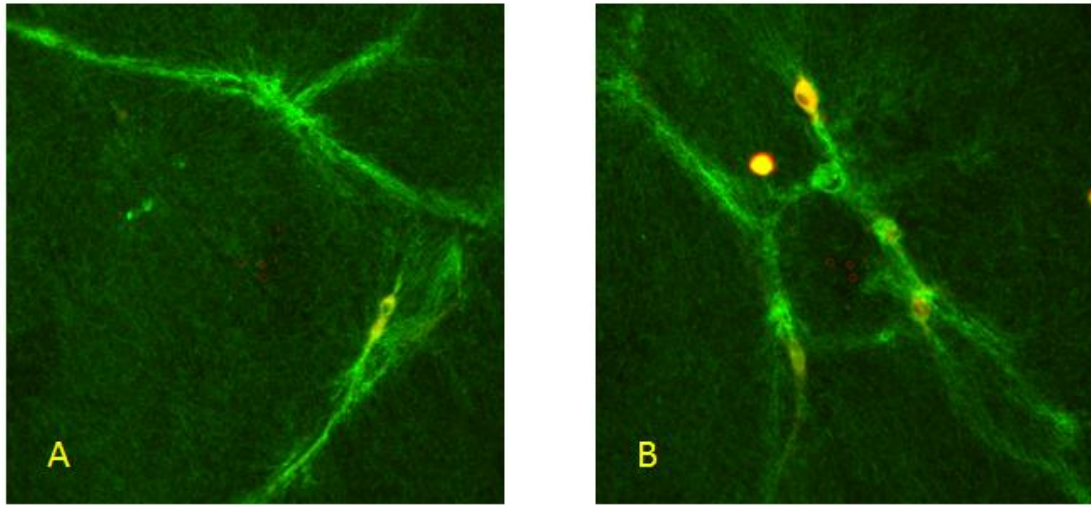


**Figure 4- 6 Collagen remodeling and Connective network of cells.**

Both vinculin-transfected cells (red) and non-transfected (green) cells were connected to each other through collagen fibers(A). Observations also suggested that the clusters of cells formed a ring-like structural network distributed throughout the ETCs. We hypothesize that this is a central mechanism of remodeling in ETCs, and that the density and alignment of collagen fiber bundles will correlate with the size and replacement time constants associated with focal adhesions.

### **4.3.3 FPR Results**

Focal adhesion dynamics in ETCs were assayed using FPR to test the hypothesis that larger and more stable focal adhesions are associated with the early stages of ETC remodeling. Although the hypothesis could not be tested in full, a framework was developed for doing so. The premise is that FA remodeling, observed as changes in time constants and total recovery of fluorescence, would change as ETCs became

increasingly remodeled, with the degree of remodeling quantified by the density and organization of the collagen fiber network in the vicinity of a FA.

Typical data for fluorescence recovery are shown in Figure 4-1. The typical fluorescence  $f(t)$  of a photobleached patch within or containing a focal adhesion would drop from a fairly steady, pre-photobleaching baseline value, then recover slightly and decay (blue line, Figure 4-1); the blue curve represents the recovery of fluorescence intensity within a region of interest that has been photobleached through a rapid ( $\sim 1$ s total duration) series of relatively intense laser pulses. The curve could be interpreted by correcting for the imaging-induced photobleaching observed in a similar focal adhesion patch within the same cell that did not experience the rapid series of relatively intense laser pulses (red line, Figure 4-1). The idea here is that the imaging process, which involves less-intense but nevertheless repeated application of the same laser, reduces fluorescence intensity from image to image in a way that often followed a clean exponential, but an exponential that differed from cell to cell. To correct for this, the “raw FPR curve” was scaled by this latter “photobleaching curve” to produce the “correction FPR” curve that was analyzed using a fitting algorithm and Equation (1) (green line, Figure 4-1).

This procedure was not free of challenges, and some photobleaching curves or raw FPR curves showed evidence of a change of time constant after an interval of imaging. This might be evident in the example shown in the photobleaching curve (red curve) in Figure 4-1. Any of a number of phenomena could lead to this, and one that will be

described in detail in the discussion below is viscoelastic relaxation or remodeling of the ETC in which the cell is embedded. Unlike FPR on cells that adhere to 2D substrates, motion due to such effects may be a central feature of cells on a 3D ETC.

Fortunately, we were able to identify guidelines for determining when such fits were adequate. The central idea is that, by identifying whether the long time constant associated with gradual signal decay in Equation (1) is very long, we can determine whether the correction curve is adequate: for a very good correction for photobleaching, the long time constant  $\tau_3$  should be very large compared to other time constants. We present these data as being of two different types in the following: data for which gradual decay occurred (Type I) and photobleaching might not have been well accounted for by our methods, and data for which  $\tau_3$  was effectively infinite compared to other time constants (Type II).

Initial FPR fitting data are shown in Tables 4-1 and 4-2 for two types of trends observed in experiments. The variation between experiments was very large. For Type I curves, time constants  $\tau_1$  and  $\tau_2$  were nearly identical for three of the six tests, indicating that only a single recovery process was active over the timescales involved in the experiment. Recovery fractions  $B$  and  $C$  were also very close in these cases. The time constants  $\tau_3$  associated with the slow decay were close to 90 seconds in four of the cases, but were significantly slower or faster in the other two. A “representative” curve is shown in Figure 4-7 for the average values of parameters in Table 4-1.

**Table 4- 1 Type I curve fitting parameters**

	$\tau_1(s)$	$\tau_2(s)$	$\tau_3(s)$	A	B	C
1	0.258	0.052	87.7	0.580	0.053	0.082
2	0.754	0.753	185.	1.01	0.079	0.079
3	0.592	0.588	77.5	1.01	0.103	0.109
4	0.503	0.501	90.8	0.722	0.145	0.141
5	0.135	0.135	82.8	0.687	0.072	0.073
6	23.4	0.109	18.4	2.07	0.638	0.111
Average	4.27	0.356	90.4	1.01	0.182	0.099
Standard deviation	9.35	0.295	53.6	0.546	0.226	0.026

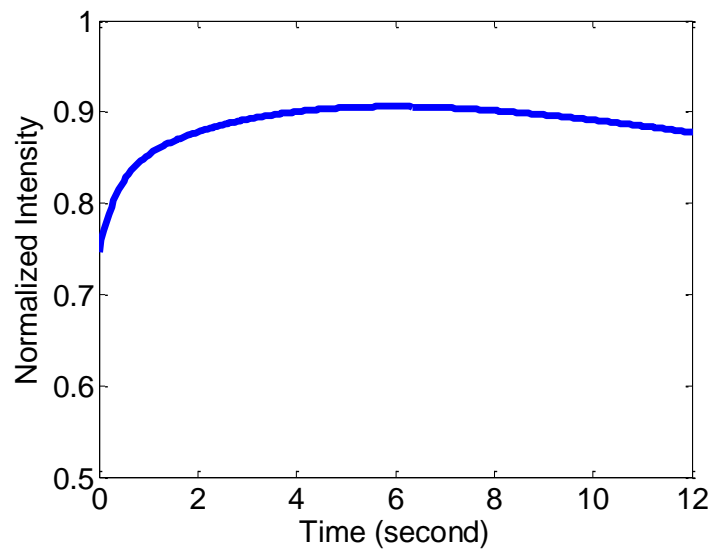


**Figure 4- 7 Type I curve of FPR**

A typical “Type I” FPR recovery curve, generated from the average parameter values in Table 4-1 for vinculin FPR obtained for fits of the character.

$$f(t) = A(1 - Be^{-t/\tau_1})(1 - Ce^{-t/\tau_2})e^{-t/\tau_3} .$$

Horizontal axis is time in seconds;

vertical axis is normalized fluorescence intensity.

For Type II curves, time constants  $\tau_1$  and  $\tau_2$  were significantly different in all seven tests, indicating that recovery processes were active.  $\tau_3$  was effectively infinite, suggesting that the photobleaching correction was very accurate in these cases, or that, if photobleaching did occur, it was counteracted by some other process, as discussed below in the context of the “Type I” results. A “typical” curve, generated from the fitting function and the average of data in Table 4-2, is shown in Figure 4-8.

**Table 4- 2 Type II curve fitting parameters.**

	$\tau_1$ (s)	$\tau_2$ (s)	$\tau_3$ (s)	A	B	C
1	3.36	0.366	$9.39 \times 10^8$	0.864	0.083	0.083
2	3.20	2.48	$1.22 \times 10^8$	1.07	0.072	0.071
3	0.452	0.075	$7.24 \times 10^8$	1.11	0.132	0.123
4	0.753	0.061	$4.77 \times 10^7$	1.14	0.137	0.162
5	1.76	0.556	$1.64 \times 10^8$	0.154	0.726	0.100
6	0.582	0.113	$2.43 \times 10^9$	0.715	0.133	-0.007
7	1.81	0.231	$4.94 \times 10^8$	0.784	0.075	0.074
Average	1.70	0.555	$1.91 \times 10^8$	0.835	0.194	0.087
Standard deviation	1.21	0.868	$3.40 \times 10^9$	0.343	0.236	0.052

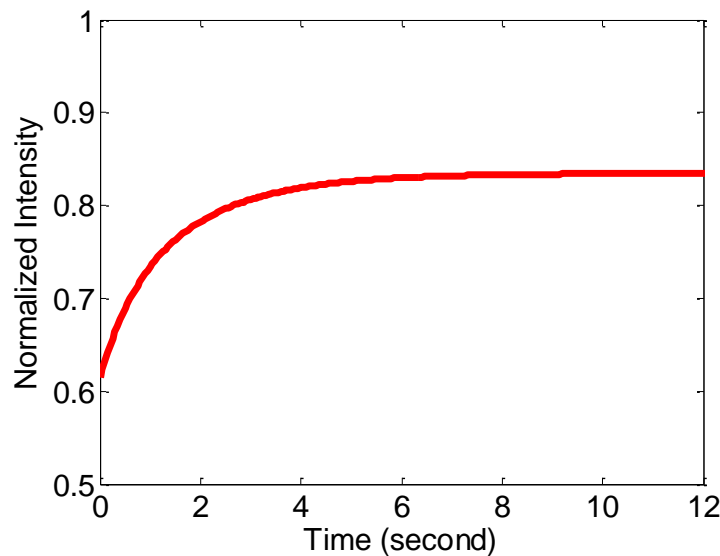


**Figure 4- 8 Type II curve of FPR**

A typical “Type II” FPR recovery curve, generated from the average parameter values in Table 4-2 for vinculin FPR obtained for fits of the character

$$I(t) = A(1 - B e^{-t/\tau_1})(1 - C e^{-t/\tau_2}) e^{-t/\tau_3} .$$
 Horizontal axis is time in seconds;

vertical axis is normalized fluorescence intensity.

## 4.4 Discussion

Studies on focal adhesion structure and regulation have shown that the components of focal adhesions are diverse and include scaffolding molecules, GTPases, and enzymes proteases, and lipases.(Wozniak, Modzelewska et al. 2004). Molecules at focal adhesions regulate various cell behaviors including integrin activity, turnover of focal adhesions, cell migration, mechano-sensing and proliferation. We focused on vinculin because of its known relationship to cell migration and mechano-sensing.

Focal adhesions are seen commonly when cells are in 2D culture. However, when cells are embedded in a 3D matrix, the sizes and the compositions of FAs are found to be different from those seen in a 2D environment. Here we illustrated that focal adhesions can be observed in the tissue-constructs-like button gels or ETCs. The shape of focal adhesions in the button gels was much more like in the 2D scenario. The shape of focal adhesions in ETCs is much rounder than the elongated patches seen in 2D culture. The large patches of FAs rarely coincide with the F-actin patches seen in the previous chapter, suggesting that F-actin patches are not structural elements but rather repositories of F-actin.

Although a qualitative observation emerged from this chapter that focal adhesions are large only during an intermediate, early stage of remodeling, a quantitative measure of this was not found. However, a system was developed whereby this can be quantified in the future. The ETC culture system shows clear and large focal adhesions, as evidenced by dual transfection. Photobleaching of these focal adhesions resulted in either one or two recovery time constants. In “Type I” cases, a third time constant was observed that was very long and on the order of time constants that are reasonable for viscoelastic relaxation of ETCs, about 90 seconds. The possibility exists that “Type I” cases displayed artifacts associated with viscoelastic relaxation of the ETC, or that in these cases the photobleaching correction was not adequate. The photobleaching correction in “Type II” cases seems to have been very good.

This chapter culminated in two culture systems in which large focal adhesions can be observed in a 3D environment, and in which FPR can be performed to uncover the replacement dynamics of these focal adhesions. The following chapter will describe future work that can determine the stability of these FAs over time, and allow interpretation of such data in the context of work on 2D systems (Wolfenson, Lubelski et al. 2009).

## 4.5 References

- Burridge, K. and L. Connell (1983). "Talin: a cytoskeletal component concentrated in adhesion plaques and other sites of actin-membrane interaction." *Cell Motil* 3(5-6): 405-417.
- del Rio, A., R. Perez-Jimenez, et al. (2009). "Stretching single talin rod molecules activates vinculin binding." *Science* 323(5914): 638-641.
- Fraley, S. I., Y. Feng, et al. (2010). "A distinctive role for focal adhesion proteins in three-dimensional cell motility." *Nat Cell Biol* 12(6): 598-604.
- Geiger, B. (1979). "A 130K protein from chicken gizzard: its localization at the termini of microfilament bundles in cultured chicken cells." *Cell* 18(1): 193-205.
- Geiger, B. and A. Bershadsky (2002). "Exploring the neighborhood: adhesion-coupled cell mechanosensors." *Cell* 110(2): 139-142.
- Hirata, H., H. Tatsumi, et al. (2008). "Mechanical forces facilitate actin polymerization at focal adhesions in a zyxin-dependent manner." *J Cell Sci* 121(Pt 17): 2795-2804.
- Hynes, R. O. (1987). "Integrins: a family of cell surface receptors." *Cell* 48(4): 549-554.
- Kanchanawong, P., G. Shtengel, et al. (2010). "Nanoscale architecture of integrin-based cell adhesions." *Nature* 468(7323): 580-584.
- Kubow, K. E. and A. R. Horwitz (2011). "Reducing background fluorescence reveals adhesions in 3D matrices." *Nat Cell Biol* 13(1): 3-5; author reply 5-7.
- Lazarides, E. and K. Burridge (1975). "Alpha-actinin: immunofluorescent localization of a muscle structural protein in nonmuscle cells." *Cell* 6(3): 289-298.
- Levental, K. R., H. Yu, et al. (2009). "Matrix crosslinking forces tumor progression by enhancing integrin signaling." *Cell* 139(5): 891-906.
- Paszek, M. J., N. Zahir, et al. (2005). "Tensional homeostasis and the malignant phenotype." *Cancer Cell* 8(3): 241-254.
- Sawada, Y., M. Tamada, et al. (2006). "Force sensing by mechanical extension of the Src family kinase substrate p130Cas." *Cell* 127(5): 1015-1026.
- Shikata, Y., A. Rios, et al. (2005). "Differential effects of shear stress and cyclic stretch on focal adhesion remodeling, site-specific FAK phosphorylation, and small GTPases in human lung endothelial cells." *Exp Cell Res* 304(1): 40-49.
- Wang, J. H. and B. P. Thampatty (2006). "An introductory review of cell mechanobiology." *Biomech Model Mechanobiol* 5(1): 1-16.
- Wolfenson, H., Y. I. Henis, et al. (2009). "The heel and toe of the cell's foot: a multifaceted approach for understanding the structure and dynamics of focal adhesions." *Cell Motil Cytoskeleton* 66(11): 1017-1029.
- Wolfenson, H., A. Lubelski, et al. (2009). "A role for the juxtamembrane cytoplasm in the molecular dynamics of focal adhesions." *PLoS One* 4(1): e4304.
- Wozniak, M. A., K. Modzelewska, et al. (2004). "Focal adhesion regulation of cell behavior." *Biochim Biophys Acta* 1692(2-3): 103-119.



## Chapter 5 : Future Work

This dissertation presented a system for evaluating the effects of mechanical loading on the shape and structure of myofibroblast cells, their cytoskeletons, and their adhesions to the ECM. The fibroblast-populated collagen lattices employed, ETCs, are an attractive model tissue for *in vitro* studies of cell behavior and for quantifying the fundamental biophysics underlying growth and remodeling of bio-artificial tissues. In ETCs, cell constantly remodel their cytoskeletons and lipid membranes to sense the environment and carry out critical tasks, such as recognizing other cells, obtaining nutrients or sorting proteins. Because membranes are fluid and intrinsically disordered, investigating these and other life-sustaining processes in detail has always been difficult. This dissertation presented a mechanism for quantifying cytoskeletal and whole-cell dynamics in response to mechanical stretch of the cellular environment.

In Chapter 2, transfected cells were studied to investigate the dynamics of F-actin in the cellular cytoskeleton in response to mechanical stretches. In this testing environment, we illustrated the dynamics and formation of stress fibers, which leads to active contraction, changes in cellular morphology, and retraction of cellular processes. The results indicate how cells respond and alter structures of cytoskeleton in the 3D mechanically induced environment. The fundamental quantitative observations of Chapter 2 involved real-time imaging of myofibroblasts subjected to mechanical stretch. While, in the ensemble sense, myofibroblasts respond to mechanical loading by a highly repeatable fluidization of the actin cytoskeleton followed by both rapid and gradual

regimes of recovery, the work presented in Chapter 2 showed that at the level of individual cells these ensemble behaviors derive from a diversity of responses. Nevertheless, some guiding principles emerged. First, three classes of cytoskeletal responses were observed: fluidization, fluidization followed by reinforcement, and reinforcement. In no instance did mechanical stretch lead to a situation in which fluidization followed reinforcement. Qualitatively, several new observations emerged as well. Stress fibers were shown to result from mechanical stretch in 3D for the first time. Actin patches that had been observed previously in the work of Nekouzadeh et al. (2008) were shown to be active, dynamic players in cytoskeletal dynamics, and appeared to function as reservoirs of F-actin from which stress fibers could be drawn, and into which F-actin assembled following disassembly of a stress fiber. Cells were shown to reorient in the direction of stretch incrementally by withdrawing processes perpendicular to the direction of stretch, and developing stress fibers parallel to the direction of stretch. Although a tremendous effort was made to measure a maximum force or strain tolerance for cells or stress fibers, these efforts were not successful. This is an important area of inquiry for the future.

In Chapter 3, these phenomena were explored at the levels of entire cells stained with a cytoplasmic dye. Cell Tracker was utilized to monitor cellular behaviors in response to mechanical stimuli. Again, process withdrawal was observed perpendicular to the direction of stretch, and process extension nominally in the direction of stretch. Membrane retraction dynamics were measured for processes that retracted, and were found to match the retraction rates of stress fibers imaged using the techniques of

Chapter 2. We calculated time constants in response to different level of stretch. The time constants associated with process retractions were very slow compared to neutrophil tether retraction rates observed by Jin-yu Shao and co-workers, suggesting that cytoskeletal elements and cellular cytoplasm were strong contributors to these retraction rates. However, because of the diverse and nonlinear viscoelastic characteristics of cells, distinguishing passive responses due to external stimuli from active responses due to cellular contraction is challenging.

In Chapter 4, we proved the existence of focal adhesions in both button gels and ring shaped ETCs. Qualitative observations suggested that the sizes of focal adhesions varied with the degree of remodeling within ETCs. This leads to a hypothesis that focal adhesions are related to mechanical stretch, and that the composition or stability of focal adhesions complexes evolves throughout the remodeling process. Therefore, it is promising to investigate the dynamics of focal adhesions at different time points and quantify the dynamics of focal adhesions during stretches. Although the dissertation ended without a conclusive characterization of these features, a system was developed in which they may be investigated in the future. A recently constructed ultra-fast photobleaching system will be of particular value for these studies.

The future work in this area falls in to two categories: the cell level and the issue level. At the cell level, the study begun in Chapter 4 can be completed in a straightforward way. Cells transfected with vinculin-GFP can be employed to measure focal adhesion dynamics via FPR and thereby establish the ratio between immobile and

mobile components of focal adhesions in 3D. At the tissue level, modeling, simulation, and imaging of the remodeling process of cells based on connections of cells to one another is particularly attractive as a potential way of cutting through some of the variability observed throughout the work in this dissertation. The observations that cells establish a network to link each other is a compelling pathway by which ETC stretch of a single magnitude can produce a family of responses in cells within that ETC. Correlation of focal adhesion dynamics and size with the degree of collagen remodeling around the focal adhesion is possible with the equipment developed. Although this will be challenging, another long-term possibility is to use the stretching equipment developed to quantify the variations of focal adhesions over time in response to mechanical stimuli. Much work will be needed to track a region of interest during viscoelastic relaxation following such stretches. However, the protocols and equipment developed in this dissertation offer a powerful platform from which studies can be pursued in the future.

# Curriculum Vita

**Sheng-Lin Lee**

**Place of Birth** Taipei, Taiwan (R.O.C.)

**Education** **National Cheng Kung University**, Tainan City , Taiwan (R.O.C.)

M.S., Biomedical Engineering, 1996

Thesis: Biomechanics of Slips and Falls in Healthy Young Adults

**Washington University in Saint Louis**

M.S., Biomedical Engineering, 2008

D.Sc., Mechanical Engineering, 2011

Dissertation : “ Cellular and Cytoskeletal Responses of Myofibroblasts in Three Dimensional Culture to Mechanical Stretch”

August 2011